Prepublished copy

Nature Environment & Pollution Technology

This is a peer-reviewed prepublished version of the paper to be published in Vol. 25, No. 4, December 2026 issue

(Original Research)

Integrated Electrocoagulation-Adsorption Using Thermally Activated Bentonite for Pb, Cd, and Ni Removal from Laboratory Wastewater

Muhrinsyah Fatimura[1,3], Tuty Emilia Agustina[2]†, Susila Arita[2], Elda Melwita[2], Rully Masriatini[3] and Nurlela[3]

[1] Engineering Science Doctoral Program, Faculty of Engineering, Sriwijaya University, Jl. Palembang - Prabumulih KM.32 Indralaya, Ogan Ilir 30662, South Sumatra, Indonesia

[2] Chemical Engineering Department, Faculty of Engineering, Sriwijaya University, Jl. Palembang - Prabumulih KM.32 Indralaya, Ogan Ilir 30662, South Sumatra, Indonesia

[3] Chemical Engineering Study Program, Faculty of Engineering, PGRI University Palembang Jl. Jend. A. Yani Lorong Gotong Royong, 9/10 Ulu, Kec. Seberang Ulu II, Palembang City 30116, South Sumatra, Indonesia

† Corresponding author: Tuty Emilia Agustina; tuty_agustina@unsri.ac.id

Key Words	Electrocoagulation-adsorption, Thermally activated bentonite, Real laboratory wastewater, Heavy metal removal, Hybrid treatment system
DOI	https://doi.org/10.46488/NEPT.2026.v25i04.D1932 (DOI will be active only after the final publication of the paper)
Citation for the Paper	Fatimura, M., Agustina, T.E., Arita, S., Melwita, E., Masriatini, R. and Nurlela, N., 2026. Integrated electrocoagulation-adsorption using thermally activated bentonite for Pb, Cd, and Ni removal from laboratory wastewater, *Nature Environment and Pollution Technology*, 25(4), D1932. https://doi.org/10.46488/NEPT.2026.v25i04.D1932

ABSTRACT

Although integrated electrocoagulation-adsorption (EC-Ads) systems have demonstrated considerable potential for heavy metal removal, most previous studies have primarily focused on synthetic wastewater or single-metal systems, while comparative evaluations involving stand-alone electrocoagulation, stand-alone adsorption, and integrated EC-Ads systems using real laboratory wastewater containing multiple metals remain relatively limited This study investigated the performance of electrocoagulation alone, adsorption alone, and an integrated EC-Ads system employing thermally activated bentonite for the simultaneous removal of Pb, Cd, and Ni from real laboratory wastewater. Electrocoagulation was optimized in terms of pH, current density, and treatment time, whereas adsorption was optimized with respect to adsorbent dosage and contact time. Statistical analysis using one-way ANOVA followed by Tukey's HSD test confirmed that the operational parameters significantly affected heavy metal removal efficiencies ($p < 0.05$). The optimum operating conditions were pH 7, a current density of 0.0133 $A.cm^{-2}$, and 60 min for electrocoagulation, followed by 40 g of bentonite per 2 L of wastewater and 60 min for adsorption. Under these conditions, the integrated system achieved total removal efficiencies of 99.06% for Pb, 98.55% for Cd, and 97.34% for Ni, yielding final concentrations of 0.0521, 0.0342, and 0.0452 $mg.L^{-1}$, respectively.

The treated effluent complied with the Indonesian general wastewater discharge standards for Pb, Cd, and Ni under the investigated conditions. Electrocoagulation functioned as the primary removal stage, while adsorption served as an effective polishing step for residual metals at low concentrations. SEM-EDS, FTIR, and ICP-MS analyses supported the proposed removal mechanisms involving surface adsorption, coprecipitation, precipitation, and immobilization in solid phases. Adsorption kinetics were better fitted by the pseudo-second-order model, indicating that the adsorption behavior was more adequately described by this kinetic model under the studied conditions. Overall, these findings demonstrate that the EC-Ads system based on thermally activated bentonite is an effective and promising approach for treating real laboratory wastewater containing multiple heavy metals.

1. INTRODUCTION

Heavy metal contamination in aquatic environments is one of the most serious environmental problems because of its persistence, non-biodegradable nature, tendency to accumulate in the food chain, and potential to cause toxic effects on aquatic organisms and human health (Hikmat et al. 2023; Fei & Hu 2023). Analytical laboratory wastewater represents a particularly complex waste stream because it contains fluctuating mixtures of inorganic and organic contaminants originating from glassware washing, residual analytical reagents, sample digestion procedures, and unused standard solutions. These wastewaters frequently contain heavy metals such as Pb, Cd, and Ni at variable concentrations, which may pose environmental and health risks if discharged without adequate treatment (Sakina et al. 2023; Fei & Hu 2023).

Among these contaminants, Pb, Cd, and Ni are considered priority pollutants because of their toxicity, persistence, and bioaccumulative behavior in aquatic systems. Pb exposure may affect the nervous system, kidneys, and hematopoietic system, whereas Cd is highly toxic even at low concentrations and may accumulate in the liver and kidneys. Ni contamination is also associated with toxic effects on aquatic organisms and potential carcinogenic risks under prolonged exposure conditions. In addition, the simultaneous presence of multiple metals in laboratory wastewater may increase treatment complexity because of possible competitive interactions among dissolved ions during removal processes (Fu & Wang 2011; Zareh et al. 2024; Magdum & Itankar 2026).

Various methods have been applied for the removal of heavy metals from wastewater, including chemical precipitation, ion exchange, membrane filtration, and biological treatment. However, these methods still face several limitations when applied to complex laboratory wastewater containing mixed metals, particularly in terms of high chemical consumption, sludge generation, membrane fouling, operational complexity, and reduced efficiency at low metal concentrations (Tripathi et al. 2025; Caixeta et al. 2025).

Electrocoagulation (EC) and adsorption have emerged as promising alternatives. Electrocoagulation can generate coagulants in situ through the dissolution of sacrificial electrodes, making it effective for destabilizing contaminants and reducing the pollutant load during the initial stage of treatment (Onyenanu & Onyenanu 2025; Ammar et al. 2023; Naldi et al. 2025). Nevertheless, the application of EC as a stand-alone process still faces

several challenges, including electrode passivation, relatively high energy consumption, sludge generation, and reduced removal efficiency in wastewater with complex compositions.

On the other hand, adsorption is recognized as a simple, flexible, and effective method, particularly for removing residual dissolved metals at lower concentrations. Various adsorbents have been developed for this purpose, and bentonite has emerged as one of the most promising materials because of its high cation exchange capacity, adequate surface area, high availability, and relatively low cost (Xu et al. 2021; Merrikhpour et al. 2022). However, adsorption as a stand-alone process also has several limitations, such as adsorbent saturation, the need for regeneration, and performance decline due to the presence of competing ions in real wastewater.

However, most previous studies have mainly focused on synthetic wastewater, single-metal systems, or simplified experimental conditions that do not adequately represent the complexity of real laboratory wastewater. In addition, comparative evaluations involving stand-alone electrocoagulation, stand-alone adsorption, and integrated EC–Ads systems under real multi-metal wastewater conditions remain relatively limited (Bakry et al. 2024; Twizerimana & Wu 2024). Real laboratory wastewater generally exhibits fluctuating composition, mixed contaminants, and potential competitive interactions among dissolved metal ions, which may significantly affect treatment performance and process stability. Therefore, studies using actual laboratory wastewater are important for evaluating the practical applicability and reliability of integrated treatment systems under realistic operating conditions. A comparison of previous related studies and the novelty of the present work is summarized in Table 1.

Table 1. Comparison of previous studies on electrocoagulation–adsorption systems for heavy metal removal.

Study	Wastewater Type	Target Metal(s)	Treatment System	Main Findings	Research Gap
Al Ali et al. (2021)	Synthetic wastewater	Pb, Cd	EC–Adsorption	High heavy metal removal efficiency	Synthetic wastewater only
Bakry et al. (2024)	Industrial wastewater	Multiple heavy metals	Electrocoagulation	Effective EC performance for metal removal	No adsorption polishing stage
Twizerimana & Wu (2024)	Synthetic wastewater	Heavy metals	Hybrid treatment system	Improved removal efficiency using integrated treatment	No comparison with stand-alone systems
Present study	Real laboratory wastewater	Pb, Cd, Ni	Stand-alone EC, stand-alone adsorption, and integrated EC–Ads	Comparative evaluation under real multi-metal wastewater conditions	—

In this context, the present study evaluates the performance of stand-alone electrocoagulation, stand-alone adsorption, and an integrated EC–Ads system employing thermally activated bentonite for the simultaneous removal of Pb, Cd, and Ni from real laboratory wastewater. The study also investigates removal mechanisms through SEM-EDS, FTIR, and ICP-MS analyses, while assessing adsorption kinetics, energy consumption,

electrode consumption, and operating cost to provide a more comprehensive evaluation of the proposed treatment system.

2. MATERIALS AND METHODS

Laboratory wastewater samples from an analytical chemistry laboratory were collected from the laboratory wastewater holding tank**.** Thermally activated bentonite obtained from PT ASPROS BINAREKA (100 mesh) was used as the adsorbent. The bentonite was thermally activated at 300 °C for 2 h using a muffle furnace with a heating rate of 10 °C min^{-1}. After thermal activation, the bentonite was cooled at room temperature in a desiccator prior to use in the adsorption experiments. Aluminum electrodes (15 cm × 13 cm × 2 mm, purity ≥ 99%), a NICE DC power supply (20 V, 10 A), sulfuric acid (98%; Smartlab), and sodium hydroxide (1 M; Labchem) were used in the experiments.

2.1. Experimental design

The study was conducted experimentally using a one-factor-at-a-time (OFAT) approach as a preliminary optimization strategy to identify the dominant operational parameters under real laboratory wastewater conditions. In the electrocoagulation process, pH, current density, and treatment time were optimized sequentially, whereas adsorption was optimized in terms of bentonite dosage and contact time under the optimum electrocoagulation conditions. After establishing the optimum conditions, the performances of stand-alone electrocoagulation, stand-alone adsorption, and the integrated electrocoagulation–adsorption (EC–Ads) system were comparatively evaluated, as illustrated in Fig. 1.

All experiments were conducted in triplicate (n = 3), and the results are presented as mean ± standard deviation. Statistical differences among treatment conditions were analyzed using one-way ANOVA followed by Tukey's honestly significant difference (HSD) post hoc test at a significance level of $p < 0.05$.

.

Fig. 1: Experimental setup of the integrated electrocoagulation–adsorption system.

2.2. Stand-alone electrocoagulation process

The electrocoagulation process was optimized stepwise using a one-factor-at-a-time approach in a 2000 mL batch reactor equipped with six aluminum electrodes (Al-Al). Each electrode had total dimensions of 15 cm × 13 cm, while the immersed part of each electrode was 15 cm × 10 cm. Therefore, the effective immersed surface area used for current density calculation was 150 cm^2, calculated from the projected immersed electrode area (15 cm × 10 cm). The inter-electrode spacing was maintained at 2 cm, and 2 L of laboratory wastewater was treated in each experimental run.

The initial pH of the wastewater was measured using a calibrated pH meter and adjusted to 3, 5, 7, 9, and 11 using 98% H_2SO_4 or 1 M NaOH. Considering the corrosive nature of concentrated H_2SO_4, pH adjustment was performed carefully by controlled dropwise addition under appropriate laboratory safety procedures, including the use of personal protective equipment and continuous mixing to avoid localized acidification. After each addition, the solution was homogenized, and the pH was rechecked until the target value was reached before starting the electrocoagulation process.

After determining the optimum pH, current optimization was performed at the optimum pH with a fixed treatment time of 60 min using applied currents of 2, 4, and 6 A. The applied current was expressed as current density using Eq. (1), where the effective immersed electrode surface area was defined as 150 cm^2. Accordingly, the current density values corresponding to 2, 4, and 6 A were 0.0133, 0.0267, and 0.0400 $A.cm^{-2}$, respectively. Subsequently, treatment time was optimized at the optimum pH and current density using treatment times of 15, 30, 45, 60, and 75 min.

.

$$J = \frac{I}{A} \qquad \ldots(1)$$

where J is the current density ($A.cm^{-2}$), I is the applied current (A), and A is the effective immersed electrode surface area (cm^2).

2.3. Stand-alone adsorption process

Stand-alone adsorption was carried out in batch mode using thermally activated bentonite as the adsorbent. In each run, 2 L of wastewater was treated under continuous stirring to maintain suspension homogeneity and promote effective contact between the adsorbent and metal ions. The stirring speed was maintained at 600 rpm throughout the adsorption process. Although relatively high, this stirring condition was selected to prevent

particle sedimentation and to maintain uniform dispersion of bentonite particles during batch operation. Under these operating conditions, no significant instability of the bentonite suspension was observed throughout the adsorption process. Optimization was performed stepwise using a one-factor-at-a-time approach. In the first stage, the adsorbent dosage was varied at 20, 40, and 60 g while maintaining a constant contact time of 60 min. In the second stage, the contact time was varied at 15, 30, 45, 60, and 75 min while keeping the adsorbent dosage at the optimum value obtained from the previous stage. The optimum conditions obtained were subsequently applied in the integrated electrocoagulation–adsorption system.

.

2.4. Integrated electrocoagulation–adsorption system

In the integrated system, the wastewater was first treated under the optimum operating conditions determined for the stand-alone electrocoagulation process. The effluent obtained from electrocoagulation was then used as the influent for the adsorption stage, which was operated under the optimum conditions established for the stand-alone adsorption process. This configuration was applied to evaluate the synergistic effect of the hybrid process on heavy metal removal.

2.5. Analytical methods

An Atomic Absorption Spectrophotometer (AAS; iCE 3000 Series) was used to determine the concentrations of Cd, Ni, and Pb in the treated wastewater. Prior to analysis, the AAS instrument was calibrated using a series of standard solutions for each metal. Calibration curves were prepared using at least five concentration levels, and the linearity of the calibration was evaluated based on the coefficient of determination (R^2). The limits of detection (LOD) and limits of quantification (LOQ) were calculated from the standard deviation of the blank response and the slope of the calibration curve. Recovery tests were performed by spiking known concentrations of Pb, Cd, and Ni into wastewater samples, followed by analysis using the same analytical procedure.

The QA/QC results for Pb, Cd, and Ni analysis are summarized in Table 2. The calibration curves showed good linearity, with R^2 values higher than 0.995 for all analyzed metals. The recovery values were within the acceptable analytical range, indicating that the analytical method was reliable for determining Pb, Cd, and Ni concentrations in the wastewater matrix.

Table 2. QA/QC parameters for AAS analysis of Pb, Cd, and Ni

Metal	Calibration range ($mg.L^{-1}$)	Calibration equation	R^2	LOD ($mg.L^{-1}$)	LOQ ($mg.L^{-1}$)	Recovery (%)
Pb	0.1–5.0	y = 0.1245x + 0.0012	0.9991	0.003	0.010	98.4
Cd	0.05–2.0	y = 0.2153x + 0.0008	0.9987	0.001	0.003	97.2

Ni	0.1–3.0	y = 0.1876x + 0.0015	0.9989	0.005	0.015	96.8

Based on the initial metal concentrations and the concentrations after treatment, the heavy metal removal efficiency was calculated using Eq. (2).

$$\text{Removal Efficiency}\ (\%) = \frac{(C_0 - C_t)}{C_0} \times 100 \qquad \ldots(2)$$

where C_0 is the initial heavy metal concentration ($mg.L^{-1}$), and C_t is the heavy metal concentration after treatment at a given stage ($mg.L^{-1}$). For the integrated system, the calculation was performed for each treatment stage. In the electrocoagulation stage, C_t represents the metal concentration in the EC effluent. In the adsorption stage, C_0 represents the metal concentration in the EC effluent, while C_t represents the metal concentration in the final adsorption effluent. For the overall EC-Ads process, C_0 is the initial metal concentration in the raw wastewater, and C_t is the final metal concentration after the adsorption stage. Inductively Coupled Plasma–Mass Spectrometry (ICP-MS) was used to determine the concentrations of Cd, Ni, and Pb immobilized in the flocs and sediments generated during electrocoagulation, thereby confirming the transfer of metals from the liquid phase to the solid phase through adsorption and precipitation mechanisms. In addition to removal efficiency, the ability of bentonite to bind metals was also evaluated in terms of adsorption capacity at equilibrium. This parameter was expressed as the equilibrium adsorption capacity (q_e), which was calculated using Eq. (3).

$$q_e = \frac{(Co - Ce).V}{m} \qquad \ldots(3)$$

where C_0 represents the initial metal concentration in solution ($mg.L^{-1}$), C_e is the metal concentration at equilibrium ($mg.L^{-1}$), V is the solution volume (L), and m is the mass of adsorbent (g). The parameter q_e represents the amount of adsorbate bound to the adsorbent per unit mass of adsorbent at equilibrium ($mg.g^{-1}$).

For each experimental condition, the concentrations of Pb, Cd, and Ni were measured for each replicate run, and the corresponding removal efficiencies were calculated using Eq. (2). The results are presented as mean ± standard deviation from triplicate measurements.

For quality assurance and quality control (QA/QC), the AAS instrument was calibrated using multi-point standard solutions for Pb, Cd, and Ni before analysis. Calibration linearity (R^2), limits of detection (LOD), limits of quantification (LOQ), and recovery data were determined according to the instrument calibration and validation procedure.

2.6. Characterization of bentonite and EC sludge

Fresh thermally activated bentonite and bentonite after adsorption were characterized using SEM-EDS and FTIR. The sludge generated from the EC process was dried and analyzed using Inductively Coupled Plasma–Mass Spectrometry (ICP-MS) and FTIR to investigate the metal capture mechanisms during the electrocoagulation stage.

2.7. Kinetic, energy, and cost analyses

Adsorption kinetic analysis was carried out to evaluate the rate of adsorbate uptake by the adsorbent as a function of time and to identify the mechanisms governing the process. For this purpose, the adsorption capacity was calculated both at a given time (q_t) and at equilibrium (q_e), as expressed in Eqs. (4) and (5), respectively.

$$q_t = \frac{(C_0 - C_t).V}{m} \quad \ldots(4)$$

$$q_e = \frac{(C_0 - C_e).V}{m} \quad \ldots(5)$$

where q_t denotes the adsorption capacity at time t ($mg.g^{-1}$), while q_e represents the adsorption capacity at equilibrium ($mg.g^{-1}$). Furthermore, C_0 is the initial adsorbate concentration in solution ($mg.L^{-1}$), C_t is the adsorbate concentration at time t ($mg.L^{-1}$), and C_e is the adsorbate concentration at equilibrium ($mg.L^{-1}$). The variable V denotes the volume of the adsorbate solution (L), whereas m is the mass of adsorbent used (g).

The kinetic data obtained were analyzed using pseudo-first-order and pseudo-second-order kinetic models. In the present study, linearized forms of the kinetic equations were employed to facilitate comparative evaluation of adsorption behavior and parameter estimation. Although nonlinear fitting may reduce potential statistical bias associated with linear transformation, the linear approach remains widely applied for preliminary kinetic interpretation and comparison with previous adsorption studies.

The pseudo-first-order model is expressed in linear form, as shown in Eq. (6).

$$ln(q_e - q_t) = ln(q_e) - k_1 t \quad \ldots(6)$$

In this equation, k_1 is the rate constant of the pseudo-first-order model (min^{-1}), q_e is the adsorption capacity at equilibrium ($mg.g^{-1}$), q_t is the adsorption capacity at time t ($mg.g^{-1}$), and t is the adsorption time (min). For comparison, the adsorption behavior was also analyzed using the pseudo-second-order model, which is expressed in linear form in Eq. (7).

$$\frac{t}{qt} = \frac{t}{k2qe^2} + \frac{t}{qe} \quad \ldots(7)$$

In this equation, k_2 is the rate constant of the pseudo-second-order model ($g.mg^{-1}.min^{-1}$), q_e is the adsorption capacity at equilibrium (mg/g), q_t is the adsorption capacity at time t ($mg.g^{-1}$), and t is the adsorption time (min). The most appropriate kinetic model was determined based on the coefficient of determination (R^2) and the agreement between the experimental adsorption capacity and the model-calculated adsorption capacity.

2.8. Energy consumption

To evaluate the energy requirement during the electrocoagulation process, electrical energy consumption was calculated based on the relationship among voltage, current, operating time, and the volume of wastewater treated, as expressed in Eq. (8).

$$E = \frac{(U \times I \times t)}{V} \quad \ldots(8)$$

In this equation, E represents the electrical energy consumption during the electrocoagulation process ($kWh.m^{-3}$), U is the applied voltage (V), I is the electric current (A), t is the operating time (h), and V is the

volume of wastewater treated (m^3). All units were expressed according to the International System of Units (SI) to ensure consistency in energy consumption calculations.

2.9. Electrode consumption

In addition to energy consumption, the amount of electrode material dissolved during the process was also evaluated as an important operational parameter. Electrode consumption was calculated from the difference in electrode mass before and after the process and then normalized to the volume of wastewater treated, as shown in Eq. (9).

$$C_{\text{electrode}} = \frac{\text{m\_initial} - \text{m\_final}}{\text{V}} \quad \ldots(9)$$

Electrode consumption represents the amount of anode material dissolved during the electrocoagulation process. This value was calculated from the difference in electrode mass before and after operation and then normalized to the volume of wastewater treated, as expressed in Eq. (9). In this equation, $C_{electrode}$ is the electrode consumption ($kg.m^{-3}$), m_initial is the electrode mass before the process, m_final is the electrode mass after the process, and V is the volume of wastewater treated (m^3). Theoretically, electrode dissolution is the basis for coagulant generation in electrocoagulation; therefore, electrode consumption is an important parameter from both process and economic perspectives.

2.10. Adsorbent consumption

In the adsorption stage, material usage was also expressed as adsorbent consumption to indicate the mass of bentonite used per unit volume of wastewater treated. This value was calculated using Eq. (10).

$$\text{C}_{\text{adsorbent}} = \frac{m_{adsorbent}}{V} \quad \ldots(10)$$

In this equation, $C_{adsorbent}$ is the adsorbent consumption ($kg.m^{-3}$), $m_{adsorbent}$ is the mass of adsorbent used (kg), and V is the volume of wastewater treated (m^3). This parameter is important because, in the integrated electrocoagulation–adsorption system, adsorbent demand directly affects both the performance of the final polishing stage and the overall operating cost.

2.11. Operating cost

To assess the operational feasibility of the process, the total operating cost was calculated as the sum of the main cost components, namely electrical energy, electrode consumption, and adsorbent usage. This general relationship is expressed in Eq. (11).

$$\text{OC} = \text{C}_{\text{energy}} + \text{C}_{\text{electrode}} + \text{C}_{\text{adsorbent}} \quad \ldots (11)$$

$$\text{OC} = (\text{a} \times \text{E}) + (\text{b} \times \text{C}_{\text{electrode}}) + (\text{c} \times \text{C}_{\text{adsorbent}}) \quad \ldots (12)$$

The total operating cost was further expressed in more detail as a function of the electricity tariff, electrode price, and adsorbent price, as shown in Eq. (12). In this study, the operating cost was calculated as the sum of the electrical energy cost, electrode consumption cost, and adsorbent usage cost, as described in Eqs. (11) and (12). In these equations, OC is the total operating cost ($Rp.m^{-3}$), E is the electrical energy consumption ($kWh.m^{-3}$), $C_{electrode}$ is the electrode consumption ($kg.m^{-3}$), $C_{adsorbent}$ is the adsorbent consumption ($kg.m^{-3}$), a is the

electricity rate ($Rp.kWh^{-1}$), b is the electrode price ($Rp.kg^{-1}$), and c is the adsorbent price ($Rp.kg^{-1}$) . These equations were used to estimate the total process cost per unit volume of wastewater treated.

The operating cost estimation in this study was limited to the major direct operational components, namely electrical energy, electrode consumption, and adsorbent usage. Additional costs associated with chemical consumption for pH adjustment, sludge handling and disposal, labor, and maintenance were not included and should therefore be considered in future scale-up and techno-economic evaluations.

3. RESULTS AND DISCUSSION

The wastewater used in this study was generated from routine activities in the analytical chemistry laboratory, mainly from the washing of glassware, residual standard solutions, and sample preparation residues that potentially contained heavy metals, as shown in Table 3.

Table 3: Initial characteristics of analytical chemistry laboratory wastewater.

Parameter	Value	Unit	Analytical method
pH	6.3 ± 0.1	–	pH meter
Temperature	27.4 ± 0.2	°C	Digital thermometer
Conductivity	1.26 ± 0.03	$mS.cm^{-1}$	Conductivity meter
TDS	632 ± 5	$mg.L^{-1}$	TDS meter
DO	4.8 ± 0.1	$mg.L^{-1}$	DO meter
Turbidity	18.6 ± 0.5	NTU	Turbidimeter
TSS	11.3 ± 0.4	$mg.L^{-1}$	Gravimetric method
BOD	0.5 ± 0.1	$mg.L^{-1}$	BOD_5 method
COD	8.5 ± 0.3	$mg.L^{-1}$	Dichromate method
Pb	5.5494 ± 0.0100	$mg.L^{-1}$	AAS
Cd	2.3517 ± 0.0100	$mg.L^{-1}$	AAS
Ni	1.7007 ± 0.0100	$mg.L^{-1}$	AAS

The results are presented as mean ± standard deviation from triplicate experiments (n = 3).

3.1. Optimization of the electrocoagulation process

The optimization of electrocoagulation operating parameters was carried out to determine the most effective conditions for removing Pb, Cd, and Ni from laboratory wastewater. In this system, the initial pH, current density, and contact time were selected as the main parameters because they govern metal speciation, the rate of anode dissolution, in-situ coagulant generation, and the stability of the flocs formed during the process.

As shown in Fig. 2, the initial pH had a significant effect on the removal efficiency of Pb, Cd, and Ni. The removal efficiency increased markedly as the pH was raised from 3 to 7, indicating that acidic conditions were less favorable for heavy metal removal. At pH 3, the removal efficiencies were the lowest, at approximately 60% for Pb, 62% for Cd, and 65% for Ni. This behavior can be attributed to the high concentration of H^+ ions under strongly acidic conditions, which compete with dissolved metal ions for reactive sites and inhibit the formation of metal hydroxide species and stable coagulant flocs (Tegladza et al. 2021; Mao et al. 2023; Lu et al. 2024). When the pH was increased to 5, the removal efficiencies rose to approximately 80% for Pb, 82% for Cd, and 85% for Ni, indicating that the solution conditions had become more favorable for hydrolysis reactions and the formation of effective coagulant species.

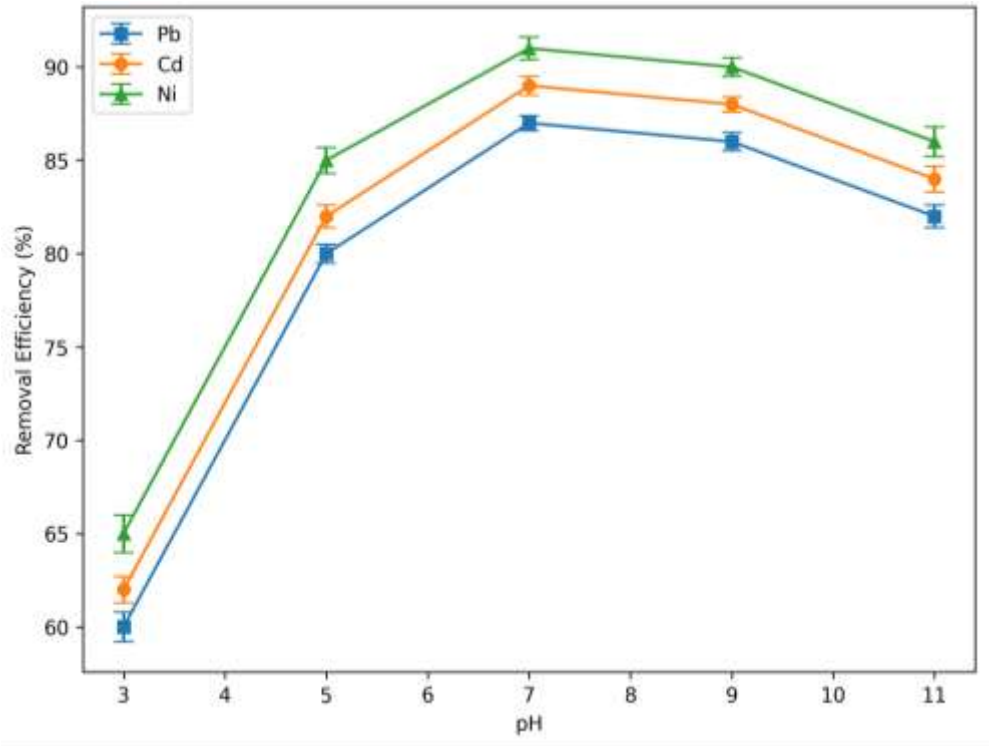

Fig. 2: Effect of pH on heavy metal removal efficiency.

The highest removal efficiencies were achieved at pH 7, reaching approximately 87% for Pb, 89% for Cd, and 91% for Ni. At near-neutral pH, aluminum hydrolysis and speciation occur within a range that is more favorable

for the formation of amorphous $Al(OH)_3$ flocs with high surface area and strong adsorptive capacity. Under these conditions, adsorption, charge neutralization, and sweep flocculation can proceed more effectively, allowing metal ions to be more readily destabilized and entrapped in the solid phase (Huang et al. 2020; Ullah et al. 2025). These results indicate that neutral pH was the optimum condition for heavy metal removal in this system, likely because of the more effective formation of amorphous hydroxide flocs and the reduced competition from H^+ ions (Tegladza et al. 2021; Lu et al. 2024). Under these conditions, dissolved metal ions can be more effectively destabilized, adsorbed, and entrapped within the floc matrix (Huang et al. 2020; Tegladza et al. 2021).

One-way ANOVA confirmed that pH significantly affected the removal efficiencies of Pb, Cd, and Ni (Pb: $F = 2386.88$, $p < 0.001$; Cd: $F = 2386.88$, $p < 0.001$; Ni: $F = 2212.50$, $p < 0.001$). Tukey's HSD post hoc test indicated that the removal efficiencies at pH 7 were significantly higher than those at pH 3, pH 5, and pH 11 ($p < 0.05$), whereas the difference between pH 7 and pH 9 was not statistically significant ($p > 0.05$). Therefore, pH 7 was selected as the optimum operating pH.

At pH 9 and 11, the removal efficiency tended to remain stable or decrease slightly, indicating that further increases in pH did not result in any meaningful improvement in performance. This behavior may be attributed to changes in aluminum speciation under more alkaline conditions, which can reduce the dominance of $Al(OH)_3$ flocs as the most effective coagulant. In addition, at excessively high pH, the increased OH^- concentration in the bulk solution and in the vicinity of the cathode may alter floc formation conditions, thereby making the sweep flocculation window less favorable and preventing metal capture efficiency from increasing proportionally (Huang et al. 2020; Matra et al. 2025).

This behavior indicates that the system reached its optimum performance under near-neutral conditions, whereas excessively high alkalinity may affect metal speciation or floc stability, thereby limiting any further improvement in removal efficiency (Mao et al. 2023; Lu et al. 2024).

Overall, these results confirm that pH 7 was the optimum condition for heavy metal removal in the system investigated. Across all pH variations, the removal efficiency followed the order Ni > Cd > Pb, indicating that Ni was the most effectively removed ion under the experimental conditions. This trend is likely related to differences in hydrolysis behavior, ionic properties, and the affinity of each metal for the hydroxide flocs or adsorptive sites (Huang et al. 2020; Tegladza et al. 2021).

As shown in Fig. 3, increasing the current density from 0.0133 to 0.0400 A.cm^{-2} resulted in a decline in removal efficiency for all metals investigated. At the lowest current density, 0.0133 A.cm^{-2}, the removal efficiencies were approximately 85% for Pb, 86% for Cd, and 89% for Ni. When the current density was increased to 0.0267 A.cm^{-2}, the removal efficiencies decreased to about 82% for Pb, 84% for Cd, and 87% for Ni. A further decline was observed at 0.0400 A.cm^{-2}, with removal efficiencies of approximately 78% for Pb, 81% for Cd, and 84% for Ni. These results indicate that 0.0133 A.cm^{-2} was the optimum current density for this system.

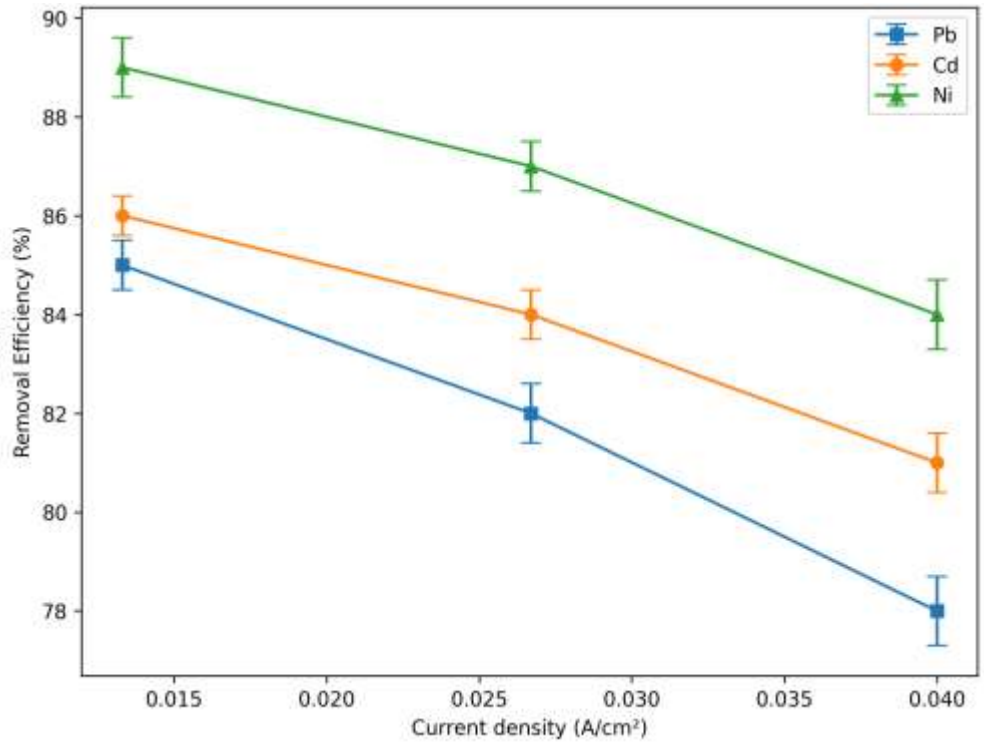

Fig. 3. Effect of current density on heavy metal removal efficiency.

One-way ANOVA also confirmed that current density significantly influenced the removal efficiencies of Pb, Cd, and Ni (Pb: $F = 231.25$, $p < 0.001$; Cd: $F = 118.75$, $p < 0.001$; Ni: $F = 118.75$, $p < 0.001$). Tukey's HSD test

showed that the removal efficiencies obtained at 0.0133 A.cm^{-2} were significantly higher than those obtained at 0.0267 and 0.0400 A.cm^{-2} ($p < 0.05$), confirming 0.0133 A.cm^{-2} as the optimum current density.

In theory, a higher current density should increase the rate of anode dissolution and in-situ coagulant generation (Ammar et al. 2023; Mao et al. 2023; Lu et al. 2024). However, in this system, increasing the current density did not improve the removal efficiency. This phenomenon may be attributed to the rapid and excessive generation of gas bubbles at higher currents, which can disrupt the formation of stable flocs and reduce the effectiveness of interactions between coagulant species and metal ions (Tegladza et al. 2021; Mao et al. 2023). At higher current densities, rapid gas bubble generation at the electrode surface may induce excessive turbulence and hydrodynamic disturbance within the reactor. Under such conditions, the flocs formed become more fragile and susceptible to breakage or re-dispersion, thereby reducing the effectiveness of sweep flocculation and metal entrapment. In addition, excessive coagulant generation may lead to local oversaturation of charged species near the electrodes, which can partially destabilize previously formed aggregates and reduce effective metal–floc interactions (Tegladza et al. 2021; Mao et al. 2023).

Furthermore, higher current density may accelerate electrode surface passivation and shorten the effective contact time between dissolved metal ions and active hydroxide flocs because of intensified bubble evolution. As a result, although higher current density theoretically increases coagulant production, the overall removal efficiency may decline because the system exceeds its optimum hydrodynamic and electrochemical operating conditions. In addition, an excessively high current density may increase local turbulence around the electrodes, causing the flocs formed to become less stable, more prone to breakage, and less likely to form larger agglomerates. Under such conditions, the system may have exceeded its effective operating range, where increased coagulant generation no longer translates into improved removal efficiency. Instead, excessive gas bubble formation and hydrodynamic disturbance may reduce the effective contact time between metal ions and electrocoagulation flocs. Furthermore, the overly rapid generation of charged species near the electrodes may also lead to partial restabilization of suspended particles, thereby reducing the net removal efficiency.

Therefore, although a higher current increases the intensity of the electrochemical process, in this system a lower current density provided a better balance among coagulant generation, floc stability, and metal capture, resulting in higher removal efficiency (Ammar et al. 2023; Tegladza et al. 2021). Accordingly, increasing current intensity does not necessarily lead to improved removal performance.

The order of removal efficiency remained consistent across all current density variations, namely Ni > Cd > Pb, indicating that Ni exhibited the highest removal affinity under the operating conditions tested.

Overall, these results confirm that current density optimization is a key factor in the electrocoagulation process, as this parameter affects not only coagulant generation but also floc stability and the efficiency of heavy metal removal (Ammar et al. 2023; Mao et al. 2023; Lu et al. 2024).

As shown in Fig. 4, increasing the contact time from 15 to 60 min resulted in a significant increase in the removal efficiency of Pb, Cd, and Ni. At 15 min, the removal efficiencies were approximately 55% for Pb, 58% for Cd, and 60% for Ni, which increased to about 70–76% at 30 min and 80–86% at 45 min. The highest removal efficiencies were achieved at 60 min, reaching approximately 85% for Pb, 87% for Cd, and 90% for Ni.

Electrocoagulation time significantly affected heavy metal removal (Pb: $F = 2956.88$, $p < 0.001$; Cd: $F = 2780.63$, $p < 0.001$; Ni: $F = 2966.25$, $p < 0.001$). Tukey's HSD analysis showed that the removal efficiencies at 60 min were significantly higher than those at 15, 30, and 45 min ($p < 0.05$), whereas the difference between 60 and 75 min was not statistically significant ($p > 0.05$). Thus, 60 min was selected as the optimum electrocoagulation time. This trend indicates that longer contact time enhances anode dissolution, promotes the formation of hydrolyzed aluminum species, and facilitates the growth of $Al(OH)_3$ flocs, thereby improving metal capture through adsorption, coprecipitation, and sweep flocculation mechanisms (Mouedhen et al. 2008; Ullah et al. 2025). At the initial stage, the availability of active sites and high binding capacity enable rapid removal, whereas increased interaction between metal ions and coagulant species further enhances removal efficiency (Ammar et al. 2023; Khan et al. 2023; Raji et al. 2023; Yang et al. 2025).

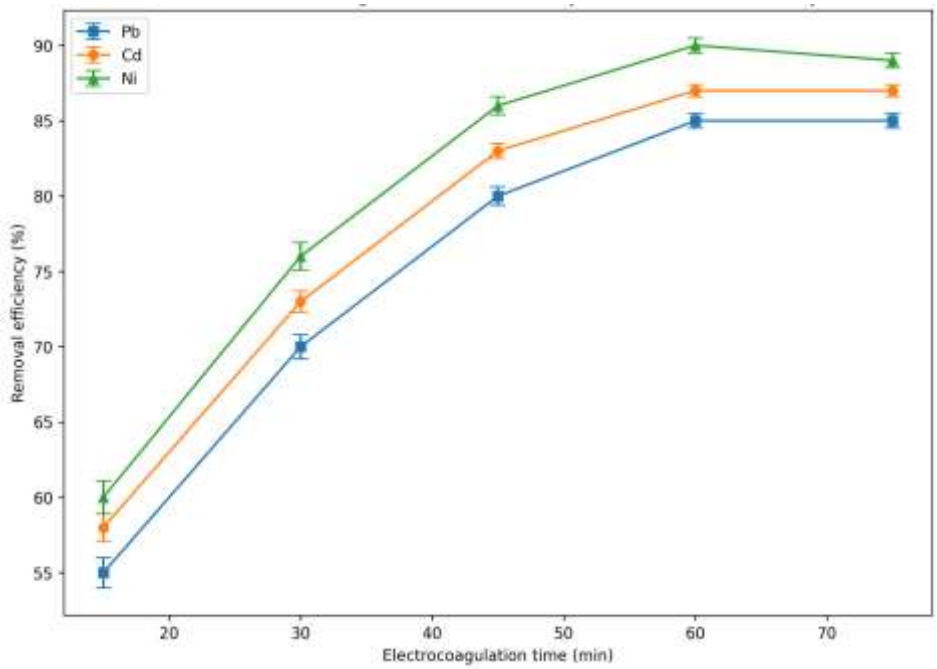

Fig. 4. Effect of Time on Heavy Metal Removal Efficiency.

However, after 60 min, most of the active sites and the system's binding capacity appeared to have been substantially utilized, so that further increases in contact time did not produce a significant improvement. The slight decline observed at 75 min may be attributed to partial desorption, redistribution of adsorbed species, or floc instability during prolonged operation.

Overall, the optimization results demonstrate that pH, current density, and contact time significantly influence heavy metal removal efficiency. Neutral pH favored effective floc formation, while lower current density improved process stability. Increasing contact time enhanced removal efficiency up to an optimum point, beyond which performance stabilized. Accordingly, the optimum electrocoagulation conditions were pH 7, current density 0.0133 $A.cm^{-2}$, and contact time 60 min. These conditions provided the best balance between coagulant generation, floc stability, and metal removal efficiency and were therefore used for subsequent integration with the adsorption process (Ammar et al. 2023; Bakry et al. 2024; Twizerimana & Wu 2024).

3.2. Optimization of bentonite adsorption

One-way ANOVA showed that adsorbent dosage significantly affected the removal of Pb ($F = 207.81$, $p < 0.001$), Cd ($F = 142.19$, $p < 0.001$), and Ni ($F = 456.25$, $p < 0.001$). Tukey's HSD test indicated that increasing the dosage from 20 to 40 g significantly improved the removal efficiencies of all three metals ($p < 0.05$), whereas the difference between 40 and 60 g was not statistically significant ($p > 0.05$). Therefore, 40 g was selected as the optimum dosage. Adsorption parameters, namely adsorbent dosage and contact time, were optimized to determine the most effective conditions for removing Pb, Cd, and Ni from wastewater using thermally activated bentonite. These parameters govern the availability of active sites, the interaction between metal ions and the adsorbent surface, and the approach to equilibrium (Fan et al. 2024; Prepilková et al. 2024). As shown in Fig. 5, adsorbent dosage had a significant effect on removal efficiency. Increasing the dosage from 20 to 40 g improved removal efficiencies from approximately 75% to 81% for Pb, 72.5% to 77.5% for Cd, and 54% to 63% for Ni. This improvement is attributed to the increase in available surface area and active binding sites, which enhances metal adsorption (Fan et al. 2024; Li et al. 2025).

Table 4. presents the adsorption capacity (qe) of thermally activated bentonite at different adsorbent dosages. The qe values decreased with increasing adsorbent dosage from 20 to 60 g. This behavior is commonly observed

in adsorption systems because increasing adsorbent mass provides more adsorption sites, while the amount of dissolved metal ions in the solution remains relatively constant. Consequently, the amount of adsorbed metal per unit mass of adsorbent becomes lower at higher adsorbent dosages.

Table 4. Adsorption capacity (qe) of thermally activated bentonite at different adsorbent dosages.

Adsorbent dosage (g)	**Pb qe ($mg.g^{-1}$)**	**Cd qe ($mg.g^{-1}$)**	**Ni qe ($mg.g^{-1}$)**
20	0.0624	0.0218	0.0098
40	0.0390	0.0136	0.0062
60	0.0265	0.0091	0.0041

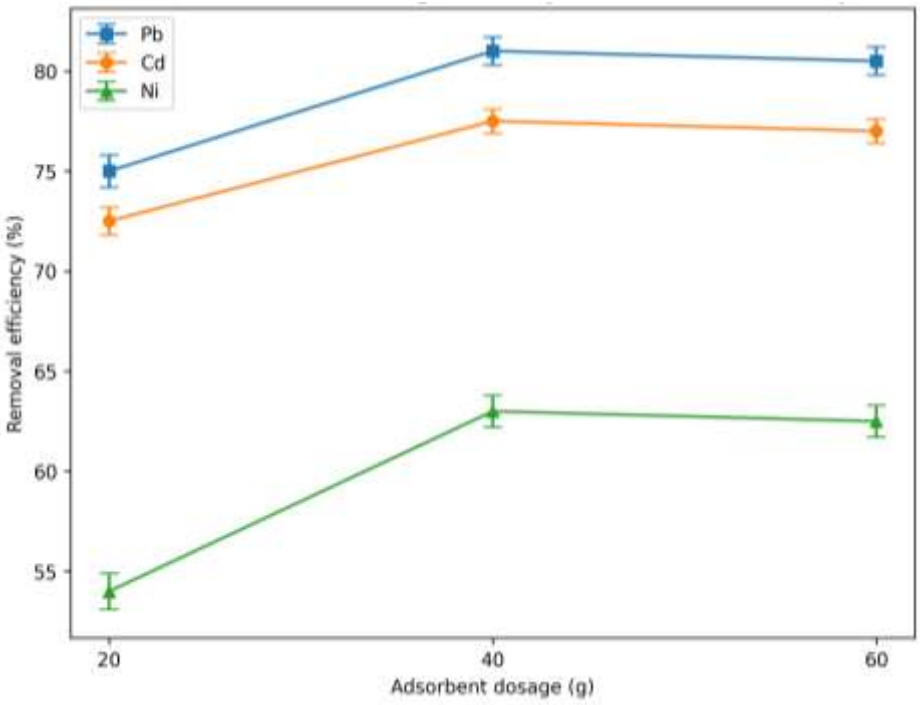

Fig. 5. Effect of adsorbent dosage on heavy metal removal efficiency.

However, further increasing the dosage to 60 g did not result in a significant improvement, with removal efficiencies remaining nearly constant or slightly decreasing. This behavior suggests that the system reached its optimum dosage at 40 g, beyond which particle aggregation and overlap may reduce effective surface area and limit accessibility of active sites. In addition, when the number of adsorption sites exceeds the available metal ions, further increases in adsorbent dosage do not proportionally enhance removal efficiency (Fan et al. 2024;

Prepilková et al. 2024). Across all dosages, the removal efficiency followed the order Pb > Cd > Ni, indicating a higher affinity of bentonite toward Pb. This trend is consistent with differences in ionic radius, hydration energy, and cation-exchange behavior on aluminosilicate surfaces (Yang et al. 2025; Li et al. 2025; Wang et al. 2024; Anna et al. 2015). Accordingly, 40 g was identified as the optimum adsorbent dosage, providing the highest removal efficiency without excessive material consumption.

Adsorption contact time also significantly affected the removal efficiencies of Pb, Cd, and Ni (Pb: $F = 1367.81$, $p < 0.001$; Cd: $F = 1073.44$, $p < 0.001$; Ni: $F = 969.38$, $p < 0.001$). Tukey's HSD analysis showed that the removal efficiencies at 60 min were significantly higher than those at 15, 30, and 45 min ($p < 0.05$), whereas the difference between 60 and 75 min was not statistically significant ($p > 0.05$). These results indicate that adsorption equilibrium was essentially reached at 60 min.

As shown in Fig. 6, contact time also significantly influenced adsorption performance. Removal efficiency increased from 30 to 60 min, reaching approximately 80.5% for Pb, 76% for Cd, and 65% for Ni. This trend reflects increased interaction between metal ions and available active sites, allowing adsorption to proceed toward equilibrium (Li et al. 2025; Wang et al. 2024).

Beyond 60 min, the removal efficiency stabilized or slightly decreased at 75 min, indicating that equilibrium had been reached and that most active sites were occupied. The slight decline may be attributed to adsorption–desorption equilibrium, redistribution of adsorbed species, or partial saturation of active sites (Yang et al. 2025; Li et al. 2025).

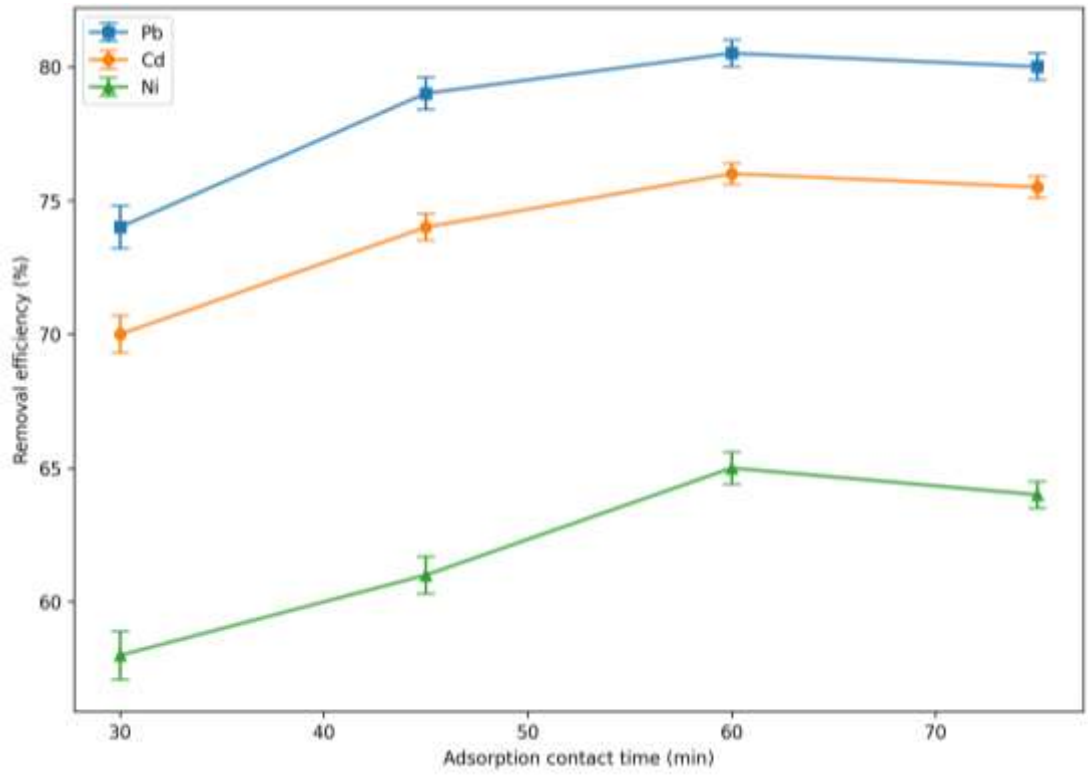

Fig. 6. Effect of Time on Heavy Metal Removal Efficiency

The removal efficiency order remained consistent (Pb > Cd > Ni) across all contact times, further confirming the higher affinity of bentonite toward Pb. Based on these results, 60 min was identified as the optimum contact time.

Overall, the optimum adsorption conditions were a bentonite dosage of 40 g and a contact time of 60 min. These conditions provided the best balance between active site availability and effective interaction time, resulting in maximum removal efficiency. The optimized parameters were subsequently used for integration with the electrocoagulation stage (Prepilková et al. 2024; Fan et al. 2024; Wang et al. 2024).

3.3. Performance of the integrated electrocoagulation–adsorption (EC-Ads) system

The final effluent contained Pb, Cd, and Ni at 0.0521 ± 0.0010 mg.L^{-1}, 0.0342 ± 0.0010 mg.L^{-1}, and 0.0452 ± 0.0010 mg.L^{-1}, respectively. These results demonstrate that the integrated EC–Ads system substantially reduced the heavy metal burden in laboratory wastewater. When evaluated against the Indonesian general discharge benchmark in Appendix XVII of Minister of Environment Regulation No. 5/2014, all three metals were below the Category I limits, indicating that the treated effluent met the applicable discharge standards for Pb, Cd, and Ni under the present treatment conditions (PERMEN, 2014).

The high removal efficiencies achieved in this study indicate that the integrated EC–Ads process has strong potential as an effective treatment strategy for laboratory wastewater containing mixed heavy metals. The combination of electrocoagulation and thermally activated bentonite adsorption provides complementary removal mechanisms that effectively reduce residual metal concentrations prior to wastewater discharge.

After the optimum conditions for each individual unit had been established, the subsequent evaluation focused on the performance of the integrated electrocoagulation–adsorption (EC-Ads) system for heavy metal removal from laboratory wastewater. Following the optimization of the individual treatment units, the performance of the integrated electrocoagulation–adsorption (EC-Ads) system was evaluated under the respective optimum conditions: pH 7, current density 0.0133 A.cm^{-2}, and contact time 60 min for electrocoagulation, and a bentonite dosage of 40 g with a contact time of 60 min for adsorption. The integrated configuration was designed such that electrocoagulation acted as the primary removal stage, reducing dissolved metal concentrations through in-situ coagulant generation and hydroxide floc formation, while adsorption served as a polishing step for the removal of residual metals (Ammar et al. 2023; Twizerimana & Wu 2024).

The concentrations of Pb, Cd, and Ni at each treatment stage are presented in Table 5, and the corresponding removal efficiencies are summarized in Table 6. The initial influent concentrations of 5.5494 mg.L^{-1} (Pb), 2.3517 mg.L^{-1} (Cd), and 1.7007 mg.L^{-1} (Ni) were reduced to 0.8324 mg.L^{-1}, 0.3057 mg.L^{-1}, and 0.1701 mg.L^{-1}, respectively, after electrocoagulation. Subsequent adsorption further reduced these concentrations to 0.0521 mg.L^{-1} (Pb), 0.0342 mg.L^{-1} (Cd), and 0.0452 mg.L^{-1} (Ni).

Table 5. Concentrations of Pb, Cd, and Ni at each stage of the EC-Ads process

Process stage	Pb (mg.L^{-1})	Cd (mg.L^{-1})	Ni (mg.L^{-1})
Initial influent (laboratory wastewater)	5.5494 ± 0.0100	2.3517 ± 0.0100	1.7007 ± 0.0100
Electrocoagulation effluent (EC effluent / adsorption influent)	0.8324 ± 0.0100	0.3057 ± 0.0100	0.1701 ± 0.0100
Adsorption effluent (final treated effluent)	0.0521 ± 0.0010	0.0342 ± 0.0010	0.0452 ± 0.0010

Table 6. Removal efficiency at each treatment stage

Process stage	Pb removal efficiency (%)	Cd removal efficiency (%)	Ni removal efficiency (%)
Electrocoagulation	85.00 ± 0.15	87.00 ± 0.37	90.00 ± 0.53
Adsorption (based on EC effluent)	93.74 ± 0.04	88.81 ± 0.04	73.42 ± 0.98
Total EC-Ads	99.06 ± 0.02	98.55 ± 0.04	97.34 ± 0.04

Table 7. presents the mass balance of Pb, Cd, and Ni throughout the integrated EC–Ads process. Based on a treatment volume of 2 L, the initial masses of Pb, Cd, and Ni were 11.10, 4.70, and 3.40 mg, respectively. During electrocoagulation, approximately 85–90% of the dissolved metals were removed from the liquid phase through adsorption onto $Al(OH)_3$ flocs, coprecipitation, and sweep flocculation mechanisms. The subsequent adsorption stage further reduced the residual dissolved metal concentrations, removing an additional 1.56 mg Pb, 0.54 mg Cd, and 0.25 mg Ni. Overall, the integrated EC–Ads system removed 10.99 mg Pb, 4.64 mg Cd, and 3.31 mg Ni, corresponding to total removal efficiencies of 99.06%, 98.55%, and 97.34%, respectively. These results confirm that the removed metals were effectively transferred from the aqueous phase to the solid phase during treatment.

Table 7. Mass balance of Pb, Cd, and Ni during the integrated EC–Ads process

Metal	Initial concentration (mg/L)	Initial mass (mg)	After EC (mg)	Final mass after Ads (mg)	Removed by EC (mg)	Removed by Ads (mg)	Total removed (mg)	Total removal (%)
Pb	5.5494	11.0988	1.6648	0.1042	9.4340	1.5606	10.9946	99.06
Cd	2.3517	4.7034	0.6114	0.0684	4.0920	0.5430	4.6350	98.55
Ni	1.7007	3.4014	0.3402	0.0904	3.0612	0.2498	3.3110	97.34

As shown in Fig. 7, the electrocoagulation stage achieved removal efficiencies of 85% for Pb, 87% for Cd, and 90% for Ni. The adsorption stage provided additional removal based on the EC effluent, with efficiencies of 93.74% for Pb, 88.81% for Cd, and 73.42% for Ni. Overall, the integrated EC-Ads system achieved high total removal efficiencies of 99.06% for Pb, 98.55% for Cd, and 97.34% for Ni.

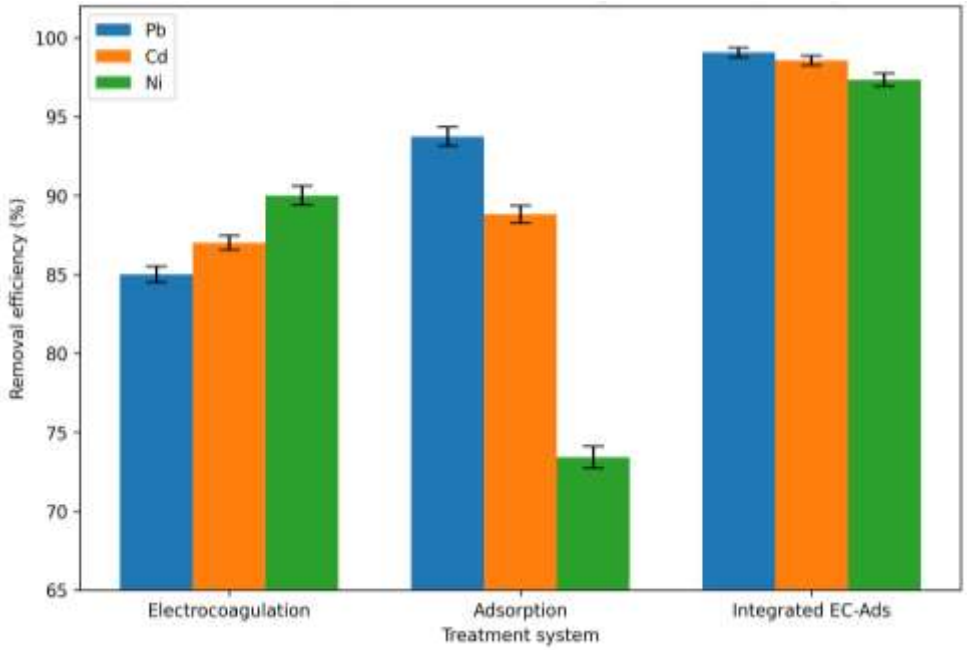

Fig. 7: Performance comparison of the electrocoagulation–adsorption system.

These findings confirm that the two processes operate in a complementary manner, where electrocoagulation effectively reduces the bulk pollutant load and adsorption enhances final effluent quality by removing residual metals at lower concentrations (Ammar et al. 2023; Twizerimana & Wu 2024). The integrated system therefore provides a more effective treatment configuration than either process alone, particularly for achieving high and consistent removal of multiple heavy metals from laboratory wastewater (Twizerimana & Wu 2024; Jo et al. 2024).

3.4. Metal removal mechanism

The mechanism of metal removal in the integrated electrocoagulation–adsorption (EC-Ads) system investigated in this study can be explained as the result of synergy between in-situ coagulant generation during the electrocoagulation stage and subsequent metal binding during the adsorption stage. During the electrocoagulation stage, aluminum dissolves at the anode to produce Al^{3+} ions (Eq. 13), while water reduction at the cathode generates OH^- ions and hydrogen gas (Eq. 14). The Al^{3+} ions undergo hydrolysis to form amorphous $Al(OH)_3$ flocs (Eq. 15), which act as effective coagulants with high surface area and strong adsorptive capacity, particularly under near-neutral pH conditions. This is consistent with the optimum performance observed at pH 7, where aluminum speciation and floc stability favor metal removal (Patel et al. 2025).

$$Al_{(s)} \longrightarrow Al^{3+} + 3\,e^- \quad \ldots(13)$$

$$3H_2O + 3\,e^- \longrightarrow \frac{3}{2}H_{2(g)} + 3\,OH^- \quad \ldots(14)$$

$$Al^{3+} + 3\,OH^- \longrightarrow Al(OH)_3\,(s) \quad \ldots(15)$$

Once formed, the $Al(OH)_3$ flocs removed Pb, Cd, and Ni through several simultaneous pathways, namely surface adsorption, charge neutralization, coprecipitation, and sweep coagulation. Schematically, these interactions can be expressed as the binding of divalent metal ions onto the floc surface (Eq. 16), whereas under locally OH^--rich conditions, the metal ions may also form sparingly soluble hydroxide precipitates (Eq. 17). Therefore, the substantial decrease in metal concentration observed during the EC stage in this study was likely not governed by a single mechanism, but rather by a combination of metal entrapment within the floc matrix, adsorption onto the surface of aluminum hydroxides, and partial precipitation. This explains why electrocoagulation was able to function as the primary removal unit, significantly reducing the pollutant load from the initial stage of treatment (Bakry et al. 2024).

$$M^{2+} + Al\,(OH)_{3(s)} \longrightarrow M\text{-}Al(OH)_{3(s)} \quad \ldots(16)$$

$$M^{2+} + 2\,OH^- \longrightarrow M\,(OH)_{2(s)} \quad \ldots(17)$$

where M^{2+} represents Pb^{2+}, Cd^{2+}, or Ni^{2+}. These combined mechanisms are consistent with the substantial reduction in metal concentration observed during the electrocoagulation stage, where metal ions were likely destabilized, adsorbed, and immobilized within the hydroxide floc matrix (Bakry et al. 2024).

Under these conditions, metal binding by bentonite may proceed through ion-exchange mechanisms (Eq. 18) and surface complexation (Eq. 19). Recent literature has also confirmed that bentonite- and clay-based materials exhibit strong metal adsorption behavior, mainly through a combination of electrostatic interactions, ion exchange, and metal coordination with active surface groups (Wang et al. 2024; Yang et al. 2025). Because the adsorption stage in this study received influent whose pollutant load had already been reduced in the EC unit, the active sites of bentonite could be utilized more effectively for the removal of residual metals at low concentrations.

$$2X\text{-}Na + M^{2+} \longrightarrow X_2\text{-}M + 2Na^{+} \quad \ldots(18)$$

$$2{\equiv}SOH + M^{2+} \rightleftharpoons ({\equiv}SO)_2M + 2H^{+} \quad \ldots(19)$$

where X denotes the cation-exchange sites on bentonite, and ≡SOH represents the active surface functional groups. Because the adsorption stage treats a pre-treated effluent with reduced metal concentration, the available active sites are utilized more efficiently for selective removal of residual metals.

Overall, the characterization data obtained provide complementary evidence for the two-stage mechanism operating in the EC-Ads system. The appearance of Pb, Cd, and Ni in the EDS spectra of bentonite after adsorption indicates that these metals were deposited on the adsorbent surface, while the changes in surface morphology observed in the SEM images suggest surface coverage and partial pore blockage by bound metal species. Furthermore, changes in the intensity and profile of the FTIR bands of bentonite after adsorption, particularly in the regions associated with O–H, H–O–H, and Si–O/Si–O–Si groups, indicate the involvement of active surface functional groups in metal binding.

During the electrocoagulation stage, the FTIR spectrum of the sludge, which exhibited dominant bands corresponding to hydroxyl groups and metal–oxygen bonds. These observations provide supporting evidence for the formation of hydrated aluminum hydroxide/oxyhydroxide flocs that may participate in adsorption, coprecipitation, and precipitation processes. In addition, the ICP-MS results, showing that most of the metal mass was transferred to the solid phase . The mass balance analysis further demonstrated that most of the removed metals accumulated in the sludge and adsorbent solids, supporting the proposed transfer of contaminants from the liquid phase to the solid phase during treatment.

The proposed removal mechanisms are further supported by the consistency between the characterization results and the mass balance analysis. SEM–EDS analysis detected Pb, Cd, and Ni in the spent bentonite and

electrocoagulation solids, demonstrating that the removed metals were retained within the solid matrix after treatment. In parallel, FTIR analysis revealed changes in hydroxyl- and silicate-related functional groups after adsorption, suggesting the participation of these active sites in metal binding. Furthermore, ICP–MS analysis confirmed that a substantial proportion of the removed metal mass was recovered in the solid phase, while the mass balance analysis quantitatively demonstrated the transfer of metals from the aqueous phase to sludge and adsorbent solids. The agreement among these independent analytical techniques provides converging evidence that metal removal occurred through a combination of adsorption, ion exchange, coprecipitation, precipitation, and sweep flocculation processes rather than through a single dominant pathway.

Although SEM–EDS, FTIR, and ICP–MS analyses cannot directly determine the exact molecular-scale binding configuration of Pb, Cd, and Ni, the combined characterization results consistently support the occurrence of adsorption, ion exchange, coprecipitation, and sweep flocculation mechanisms. The simultaneous detection of metals in the solid phase, changes in FTIR functional-group vibrations, and the observed mass transfer revealed by the mass balance analysis provide complementary evidence for the proposed removal pathways.

Therefore, the proposed mechanisms should be interpreted as being strongly supported by indirect but complementary experimental evidence rather than being conclusively proven. Future studies employing advanced surface characterization techniques such as X-ray photoelectron spectroscopy (XPS), X-ray diffraction (XRD), or other advanced spectroscopic analyses may provide more direct confirmation of the specific metal-binding mechanisms involved.

Taken together, these findings support that the integrated system operated through a complementary two-stage mechanism, namely predominant metal load reduction through floc formation during electrocoagulation, followed by the removal of residual metals through adsorption and ion exchange on thermally activated bentonite.

3.5. Characterization analysis of materials and residues

3.5.1. SEM-EDS analysis of bentonite before and after adsorption

The SEM images of fresh bentonite were interpreted as showing a layered structure with open pores. After adsorption, the surface became rougher and denser, indicating the deposition of metals or the formation of

surface complexes. EDS analysis of the spent adsorbent revealed the presence of Pb, Cd, and Ni, which were not detected in the fresh bentonite.

As summarized in Table 8, the SEM analysis showed changes in the surface morphology of bentonite before and after thermal treatment, as well as after the adsorption process. Natural bentonite exhibited an irregular structure with a rough agglomerated texture and several visible voids. After thermal activation, the bentonite surface became rougher, more fragmented, and more granular, indicating that the heat treatment modified the surface structure. After adsorption, the bentonite surface appeared denser and more agglomerated, with some pores partially covered by adsorbates. These changes suggest that thermal activation may enhance the accessibility of active sites, whereas the adsorption process leads to surface coating or pore filling by adsorbed metal ions.

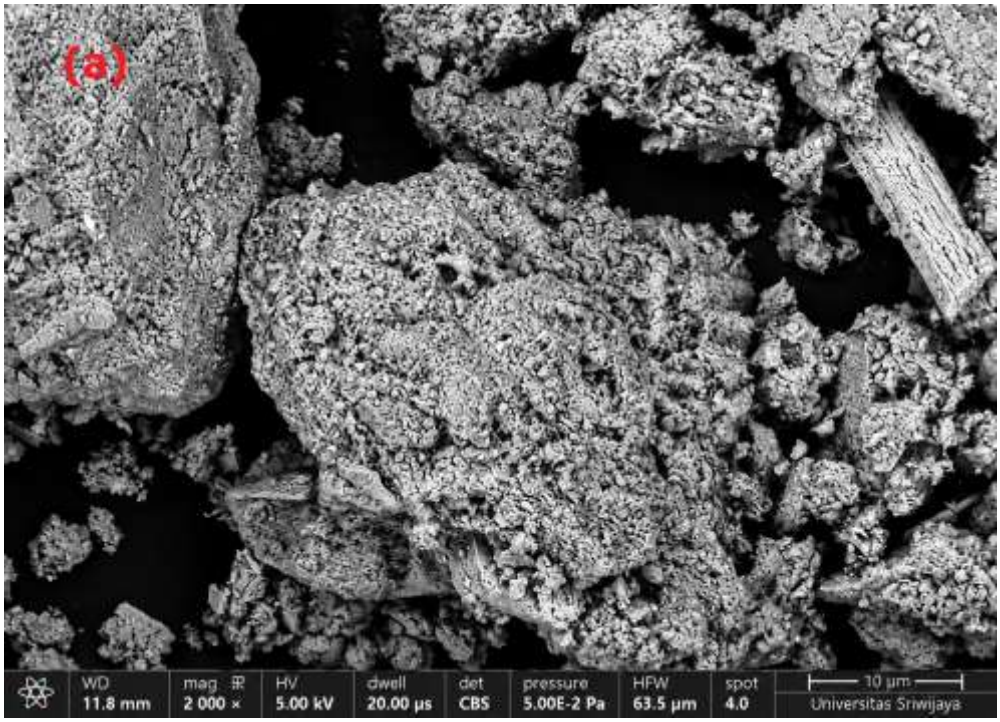

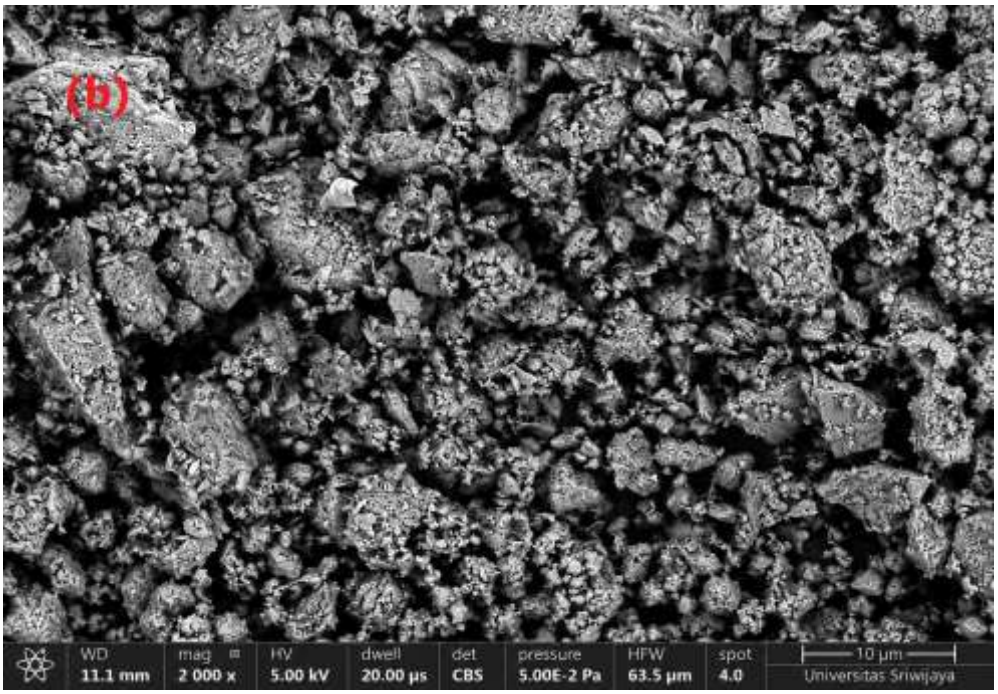

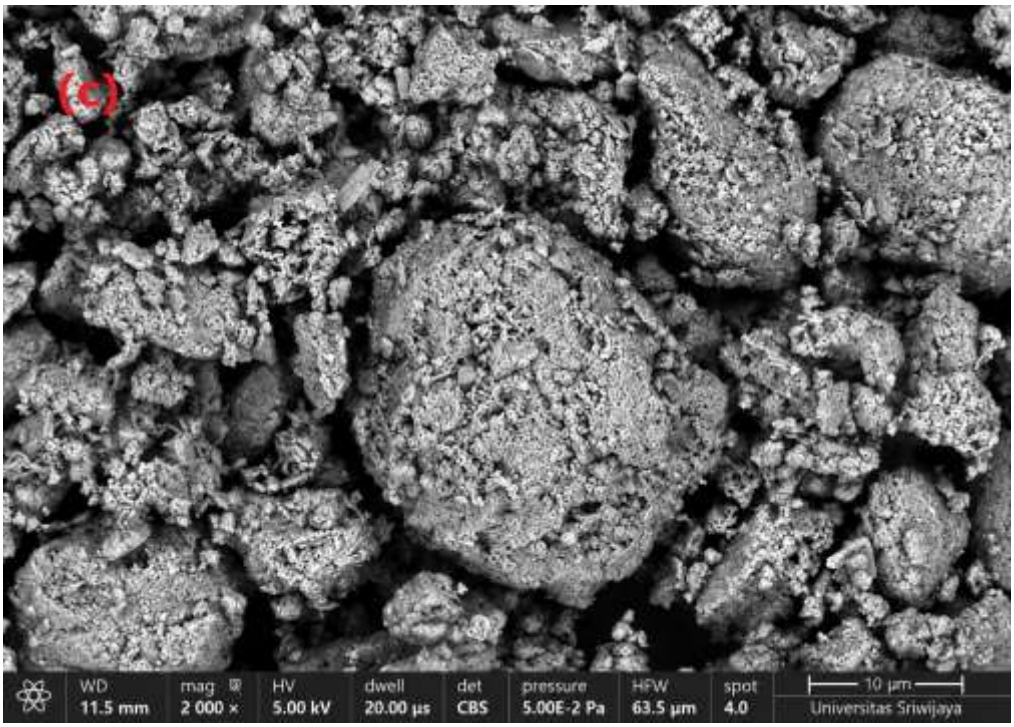

Fig. 8: SEM analysis of bentonite (a) natural bentonite, (b) thermally activated bentonite, (c) bentonite after adsorption.

Table 8. Summary of SEM-EDS results for bentonite before and after adsorption.

Parameter	Natural bentonite	Thermally activated bentonite	Bentonite after adsorption	Interpretation
Surface morphology	Irregular and porous surface with rough agglomerated texture. Visible voids and cavities are still observed.	The surface becomes rougher, more fragmented, and granular after thermal activation. Several cracks and broken particles are observed.	The surface appears denser and more agglomerated, with some pores partially covered after adsorption.	Thermal activation modifies the surface texture and may enhance surface accessibility, while adsorption leads to pore filling and surface coverage by adsorbates.

The EDS results presented in Table 9. show that both natural bentonite and thermally activated bentonite were dominated by O, Si, and Al, confirming the aluminosilicate nature of the material. After thermal activation, the composition of the major elements did not change drastically; however, the disappearance of S indicates a reduction in impurity components on the adsorbent surface. After the adsorption process, Pb, Cd, and Ni were detected at 2.6, 1.6, and 1.2 wt%, respectively, providing direct evidence that the heavy metals had been bound to the bentonite. The relative decrease in Si and Al contents after adsorption suggests that part of the active surface had been covered by metal adsorbates, while the high O content indicates that the main aluminosilicate framework remained preserved. Overall, the EDS results support that thermal activation modified the bentonite surface, whereas the adsorption process led to the binding of heavy metals onto the material surface.

Table 9. EDS analysis results of natural bentonite, thermally activated bentonite, and bentonite after adsorption.

Component	Natural bentonite Weight (%)	Natural bentonite Atomic (%)	Thermally activated bentonite Weight (%)	Thermally activated bentonite Atomic (%)	Bentonite after adsorption Weight (%)	Bentonite after adsorption Atomic (%)
C	2.8	4.7	4.6	7.5	4.3	6.9
O	50.8	62.7	51.3	62.6	50.0	61.7
Mg	1.2	0.9	1.0	0.8	0.9	0.7
Al	6.6	4.8	6.6	4.8	6.2	4.5
Si	36.3	25.5	34.4	23.9	31.6	21.9
S	2.3	1.4	–	–	–	–
Mo	–	–	2.1	0.4	1.6	0.3
Pb	–	–	–	–	2.6	0.4
Cd	–	–	–	–	1.6	0.2
Ni	–	–	–	–	1.2	0.5
Total	100.0	100.0	100.0	100.0	100.0	100.0

3.5.2. FTIR analysis of bentonite before and after adsorption

As shown in Fig. 9, the FTIR spectra of thermally activated bentonite before and after adsorption exhibited noticeable peak shifts and intensity changes, indicating interactions between heavy metal ions and functional groups on the bentonite surface. The main FTIR peak positions before and after adsorption are summarized in Table 10.

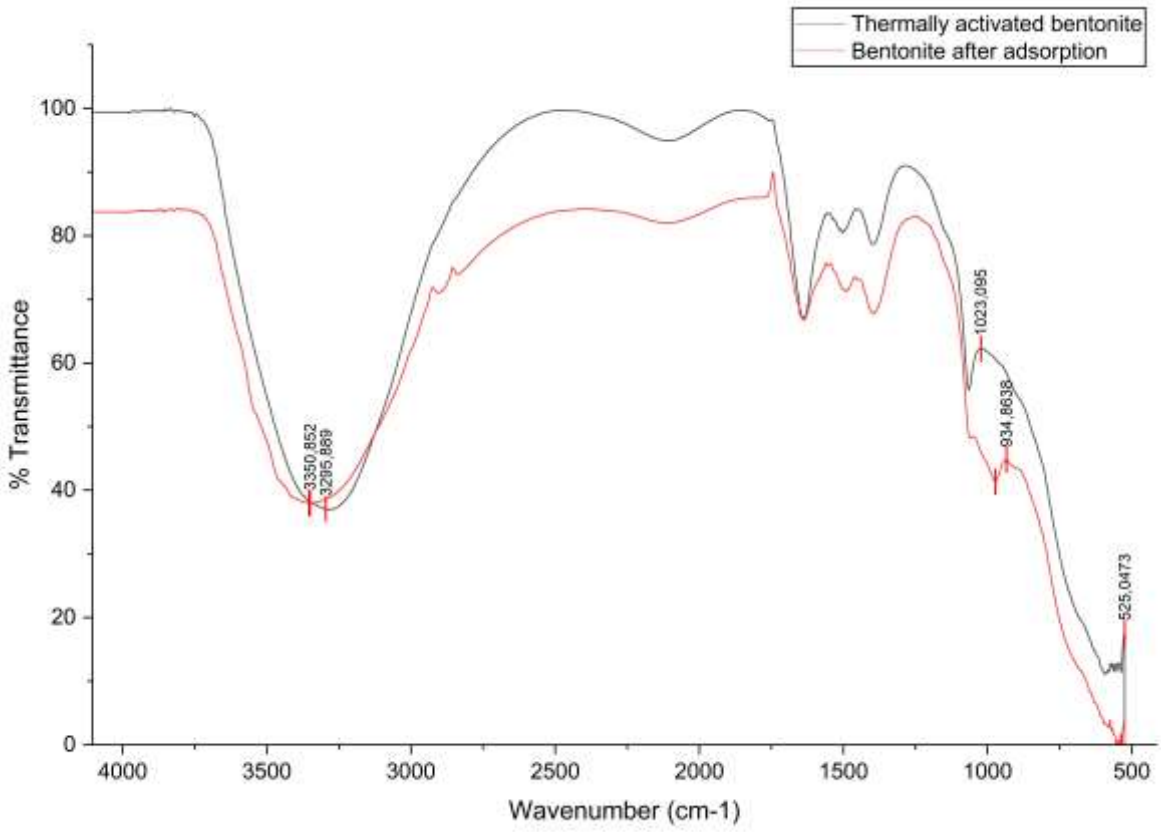

Fig. 9: FTIR spectra of bentonite before and after adsorption

Table 10. FTIR peak positions and corresponding shifts before and after adsorption

Functional group	Before adsorption (cm^{-1})	After adsorption (cm^{-1})	Shift (cm^{-1})
O–H stretching	3295.89	3350.85	+54.96
Si–O stretching	1023.10	934.86	−88.24
Si–O–Al / M–O bending	525.05	intensity change	–

As shown in Table 10, the broad absorption band assigned to O–H stretching vibrations shifted from 3295.89 cm^{-1} before adsorption to 3350.85 cm^{-1} after adsorption, corresponding to a shift of 54.96 cm^{-1}. This shift indicates the involvement of hydroxyl groups in the adsorption process and suggests the formation of surface complexes between metal ions and hydroxyl functional groups on bentonite.

In addition, the characteristic Si–O stretching vibration shifted from 1023.10 cm^{-1} to 934.86 cm^{-1} after adsorption, representing a shift of 88.24 cm^{-1}. The significant displacement of this band suggests strong

interactions between Pb^{2+}, Cd^{2+}, and Ni^{2+} ions and the aluminosilicate framework of bentonite, indicating that ion exchange and surface complexation contributed to the adsorption process.

Furthermore, changes observed in the low-wavenumber region around 525 cm^{-1}, associated with Si–O–Al and/or metal–oxygen vibrations, provide additional evidence of modifications in the local bonding environment after adsorption. Despite these spectral changes, the characteristic bands of bentonite remained present, indicating that adsorption occurred without significant destruction of the bentonite mineral structure.

Overall, the observed numerical peak shifts confirm that hydroxyl and silicate functional groups participated directly in heavy metal adsorption, supporting ion exchange and surface complexation as important removal mechanisms.

3.6. Characterization of electrocoagulation sludge

To comprehensively understand the removal mechanism and validate the fate of heavy metals (Cd, Ni, and Pb) during the electrocoagulation process, a detailed characterization of the generated sludge was carried out (Patel et al. 2025; Bakry et al. 2024). This section discusses the macroscopic appearance of the dried flocs, followed by a molecular-level investigation using Fourier Transform Infrared (FTIR) spectroscopy to identify the functional groups involved in metal binding (Rajaniemi et al. 2021).

In addition, Inductively Coupled Plasma (ICP-MS) analysis was used to quantify elemental distribution in the sludge, thereby confirming mass balance closure between the liquid and solid phases. This multi-analytical approach provides strong evidence for chemisorption and complexation mechanisms previously suggested by the kinetic and thermodynamic data.

Fig. 10 presents digital macroscopic images of the solid phase generated during the electrocoagulation process: (a) freshly formed gelatinous $Al(OH)_3$ flocs between the aluminum electrodes and (b) dried sludge obtained after electrocoagulation. The clear differences in morphology and color indicate the successful transformation of dissolved metal ions into a stable, insoluble solid matrix, consistent with the high removal efficiency (>99%) observed at pH 7.

Fig. 10. (a) Floating flocs (b) Dried flocs formed during the electrocoagulation process.

As shown in Fig. 11, the FTIR analysis of the flocs generated during the electrocoagulation process exhibited dominant absorption bands at approximately 3353.75, 1634.14, 1394.82, 973.49, and 531.58 cm^{-1}, indicating the formation of an inorganic floc matrix rich in hydroxyl groups and metal–oxygen bonds.

The broad band at 3353.75 cm^{-1} was attributed to O–H stretching vibrations, indicating the presence of surface hydroxyl groups and adsorbed water on the flocs, whereas the band at 1634.14 cm^{-1} was associated with H–O–H bending vibrations of bound water, confirming the hydrated nature of the electrocoagulation residue. Furthermore, the band at 1394.82 cm^{-1} indicates the presence of carbonate species that were likely adsorbed or incorporated into the floc structure during the process.

The band at 973.49 cm^{-1} was assigned to M–OH and/or M–O vibrations in metal hydroxide or oxyhydroxide phases, while the band at 531.58 cm^{-1} is characteristic of metal–oxygen (M–O) bonds. Overall, these spectral features confirm that the metal removal mechanism during electrocoagulation was dominated by the formation of hydrated hydroxide/oxyhydroxide flocs, which served as active sites for adsorption, coprecipitation, and precipitation, thereby enabling the effective immobilization of metal contaminants into the solid phase formed (Patel et al. 2025; Bakry et al. 2024; Harahap et al. 2024).

The removal mechanism of Pb, Cd, and Ni was elucidated by integrating the quantitative mass balance obtained from ICP-MS with molecular-level characterization by FTIR. Based on the ICP-MS data in Table 11, the initial metal masses in the aqueous phase were 11.0988 mg for Pb, 4.7034 mg for Cd, and 3.4014 mg for Ni. After the EC process, the metal masses remaining in the filtrate were 1.6648, 0.6114, and 0.3402 mg, respectively, whereas the metal masses measured in the dried sludge reached 10.6374, 4.1952, and 3.3620 mg, respectively. These data indicate that most of the metals were transferred from the liquid phase to the solid phase during the electrocoagulation process. This integrated analysis demonstrates that electrocoagulation effectively

immobilized the mixed metals through strong chemical entrapment within the hydroxide floc structure (Yazıcı 2025).

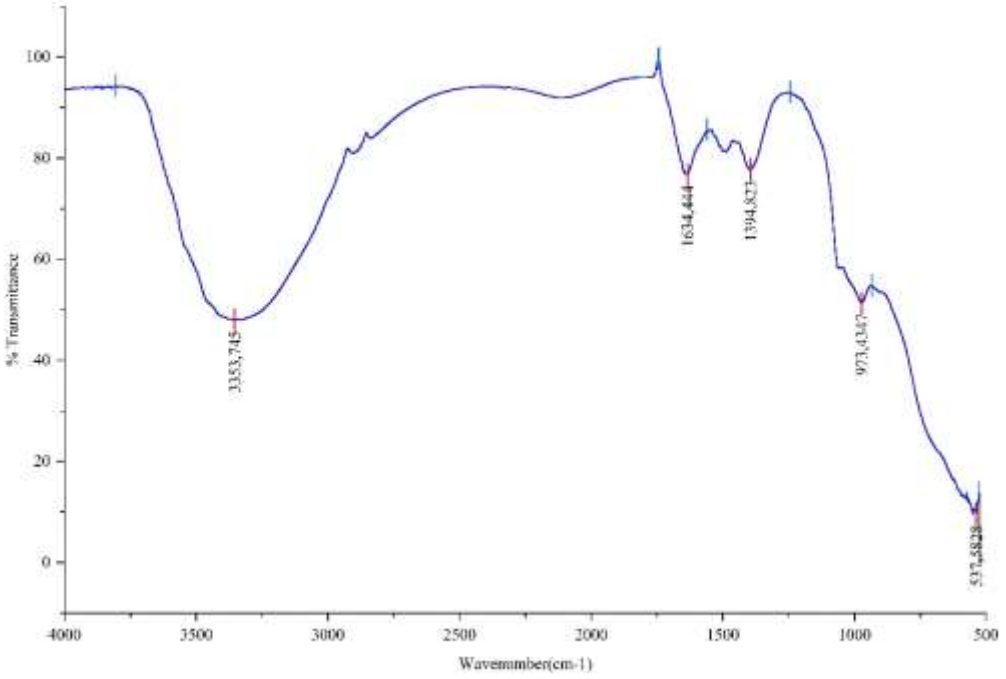

Fig. 11. FTIR analysis of flocs generated during the electrocoagulation process.

Table 11. Mass balance and elemental composition of dried sludge determined by ICP-MS analysis

Component	Parameter	Pb	Cd	Ni	Total mixture
Aqueous phase	Initial concentration, (C_0) (mg.L^{-1})	5.5494	2.3517	1.7007	9.6018
	Initial mass, (m_i) (mg)	11.0988	4.7034	3.4014	19.2036
	Final concentration after EC, (C_{EC}) (mg.L^{-1})	0.8324	0.3057	0.1701	–
	Final mass in filtrate, (m_f) (mg)	1.6648	0.6114	0.3402	2.6164
Solid phase	Dried sludge mass (g)	–	–	–	1.415
	Metal concentration in sludge, (C_s) (mg.kg^{-1})	7517.61	2964.79	2376.00	12858.40
	Metal mass in sludge, (m_s) (mg)	10.6374	4.1952	3.3620	18.1946

3.7. Adsorption kinetic analysis

3.7.1. Pseudo-first-order model

Table 12. Adsorption kinetic parameters of the pseudo-first-order model

Ion	$q_{e,exp}$ (mg.g^{-1})	$q_{e,\ calc}$ (mg.g^{-1})	k_1 (min^{-1})	(R^2)
Pb	0.44673	0.30852	0.07590	0.9902
Cd	0.17873	0.06315	0.05385	0.9846
Ni	0.11055	0.04591	0.04369	0.9974

Although the R^2 values were relatively high, the $q_{e,calc}$ values obtained from the pseudo-first-order model differed considerably from the experimental $q_{e,exp}$ values. This indicates that the model was less able to adequately represent the actual adsorption process in the bentonite system.

3.7.2. Pseudo-second-order model

Table 13. Adsorption kinetic parameters of the pseudo-second-order model

Ion	**$q_{e,calc}$ (mg.g^{-1})**	**k_2 (g.mg^{-1} min^{-1})**	**(R^2)**
Pb	0.47256	0.52795	0.9990
Cd	0.18805	1.37596	0.9990
Ni	0.11871	1.41502	0.9970

These results indicate that the pseudo-second-order model provided a better fit, as reflected by the very high R^2 values and the closer agreement between the calculated $q_{e,calc}$ and experimental values. In addition, the adsorption profile suggests rapid occupation of active sites followed by the attainment of a near-equilibrium state (Tran 2023; Vareda 2023).

Nevertheless, a good fit to the pseudo-second-order model does not directly prove that the adsorption mechanism was entirely governed by chemisorption; rather, it is more appropriately interpreted as indicating that the adsorption rate was likely influenced by surface interactions between the metal ions and the active sites of the adsorbent (Tran 2023; Vareda 2023).

As shown in Fig. 12, the adsorption capacity of thermally activated bentonite for Pb, Cd, and Ni increased with increasing contact time from 30 to 60 min and then tended to stabilize at 75 min. This pattern indicates that,

during the initial stage of adsorption, a large number of active sites were still available on the adsorbent surface, allowing metal uptake to proceed relatively rapidly, whereas after 60 min the system began to approach equilibrium (Raji et al. 2023; Tran 2023).

The maximum adsorption capacities obtained were 0.44673 $mg.g^{-1}$ for Pb, 0.17873 $mg.g^{-1}$ for Cd, and 0.11055 $mg.g^{-1}$ for Ni, respectively, giving an adsorption affinity order of Pb > Cd > Ni. As shown in Table 8, the adsorption kinetic data for all three metals followed the pseudo-second-order model with an excellent fit, as indicated by R^2 values of 0.9990 for Pb, 0.9990 for Cd, and 0.9970 for Ni.

In addition, the theoretical adsorption capacities ($q_{e,calc}$) predicted by the pseudo-second-order model were closer to the experimental values than those obtained from the pseudo-first-order model. These results suggest that metal adsorption by bentonite was predominantly governed by surface chemical interactions, such as ion exchange and complexation at the active sites of bentonite (Raji et al. 2023; Wang et al. 2024; Yang et al. 2024). However, this interpretation remains indicative, since other kinetic models, such as the intraparticle diffusion and Elovich models, were not evaluated in this study. Therefore, the possible contributions of intraparticle diffusion, boundary layer resistance, and other mass transfer steps cannot yet be fully excluded and should be investigated further in future studies (Vareda 2023; Yazidi et al. 2026).

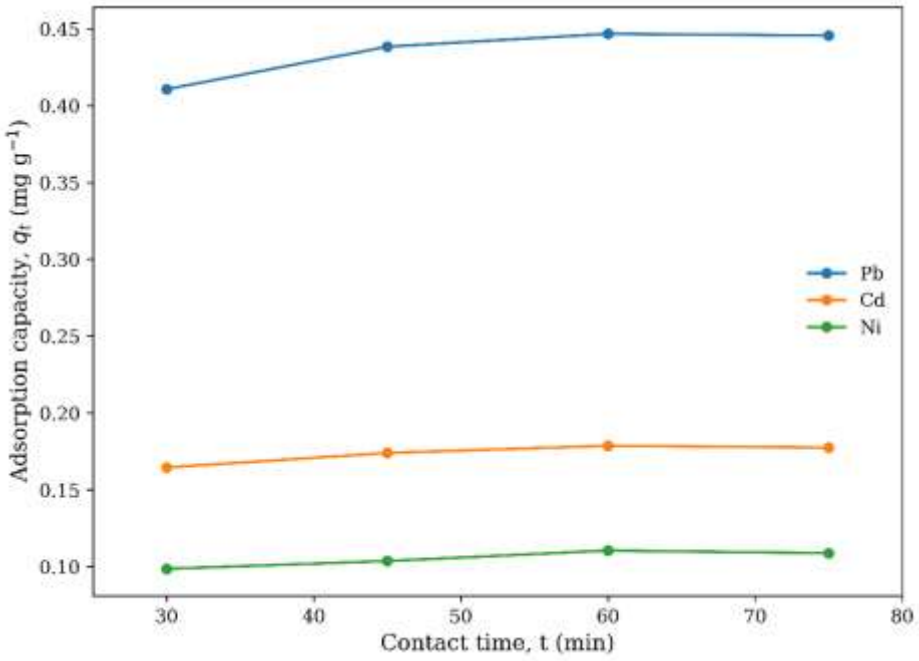

Fig. 12: Experimental adsorption kinetics of Pb, Cd, and Ni onto bentonite as a function of contact time.

3.8. Energy consumption, electrode consumption, and operating cost

As shown in Table 14, the EC-Adsorption process operated at a current of 2 A and a voltage of 10 V, with 60 min of electrocoagulation followed by 60 min of adsorption, exhibited very high removal performance for Pb, Cd, and Ni, reaching 99.06%, 98.55%, and 97.34%, respectively. The substantial reduction in residual metal concentrations indicates that the combination of the two processes was effective for removing dissolved heavy metals from laboratory wastewater.

Based on Table 10, the normalized energy, electrode, and adsorbent consumptions were 10.00 $kWh.m^{-3}$, 0.065 $kg.m^{-3}$, and 20.00 $kg.m^{-3}$, respectively. The operating cost was calculated as the sum of electricity, electrode, and adsorbent costs. An electricity tariff of Rp 1,444.7 kWh^{-1} was adopted based on the applicable tariff published by PT PLN (Persero) (PLN.2026), while the aluminum electrode and thermally activated bentonite prices were assumed to be Rp 55,000 kg^{-1} and Rp 1,250 kg^{-1}, respectively, based on local market prices. Based on these economic assumptions, the electricity, electrode, and adsorbent costs were Rp 14,447 m^{-3}, Rp 3,575 m^{-3}, and Rp 25,000 m^{-3}, respectively, resulting in a total operating cost of Rp 43,022 m^{-3}. Among all cost components, adsorbent usage contributed the largest share, followed by electrical energy, whereas electrode consumption contributed the least.

Table 14. Operating conditions and treatment performance of the EC-Adsorption process.

Parameter	Unit	Value
Wastewater volume	L	2.0
Current	A	2.0
Voltage	V	10.0
Electrocoagulation time	min	60
Adsorption time	min	60
Adsorbent dosage	$g.L^{-1}$	20.0
Initial Pb concentration	$mg.L^{-1}$	5.5494
Final Pb concentration	$mg.L^{-1}$	0.0521
Pb removal efficiency	%	99.06
Initial Cd concentration	$mg.L^{-1}$	2.3517
Final Cd concentration	$mg.L^{-1}$	0.0342
Cd removal efficiency	%	98.55
Initial Ni concentration	$mg.L^{-1}$	1.7007

Final Ni concentration	$mg.L^{-1}$	0.0452
Ni removal efficiency	%	97.34

Table 15. Resource consumption and operating cost of the EC-Adsorption process

Parameter	**Unit**	**Value**
Energy consumption	$kWh.m^{-3}$	10.00
Electrode consumption	$kg.m^{-3}$	0.065
Adsorbent consumption	$kg.m^{-3}$	20.00
Electricity cost	$Rp.m^{-3}$	14,447
Electrode cost	$Rp.m^{-3}$	3,575
Adsorbent cost	$Rp.m^{-3}$	25,000
Total operating cost	**$Rp.m^{-3}$**	**43,022**

Fig. 13 shows that increasing the current from 2 to 6 A caused a proportional increase in the energy consumption and operating cost of the EC-Adsorption system. At a current of 2 A, the process required an energy consumption of 10.00 $kWh.m^{-3}$ with a total operating cost of Rp 43,022 m^{-3}, whereas increasing the current significantly raised both the energy requirement and the treatment cost.

This pattern indicates that current is a key operating parameter governing the economic performance of the process, because energy consumption increases directly with current intensity when voltage, operating time, and wastewater volume are kept constant (Kim et al. 2025). The increase in operating cost at higher currents was mainly associated with the greater electrical energy requirement, whereas the contributions of electrode and adsorbent consumption were relatively smaller (Ebba et al. 2021; Aljaberi 2019).

These results confirm that a current of 2 A was the most favorable condition from a practical perspective, as it was able to provide high removal performance with lower energy consumption and operating cost (Uludag-Demirer et al. 2020).

Comparison with recent literature published during 2022-2025 further supports the performance of the present integrated **EC-Ads** system. In this study, the overall removal efficiencies reached 99.06% for Pb, 98.55% for Cd, and 97.34% for Ni under the optimized operating conditions. Recent electrocoagulation studies have

reported similarly high heavy-metal removal. For example, Bakry et al. (2024) reported removal efficiencies of 98-100% for several individual heavy metals, including Pb, Cd, and Ni, using aluminum-electrode electrocoagulation, whereas Aljaberi and Hawaas (2023) achieved 99.73% Pb removal and 98.54% Cd removal in a multi-metal electrocoagulation system. Shaker et al. (2023) reported Ni removal efficiencies of up to 99.9%. In this context, the removal efficiencies obtained in the present work may be considered to lie within the upper range of recent literature, particularly because the wastewater treated here was real laboratory wastewater containing multiple metals rather than a simplified single-metal synthetic solution.

From the energy standpoint, the value obtained in this study (10.00 $kWh.m^{-3}$) is also within the range reported for recent heavy-metal electrocoagulation systems, although direct comparison should be made cautiously because energy demand strongly depends on wastewater composition, reactor design, electrode material, current density, conductivity, and treatment time. Bakry et al. (2024) reported a broad electrical energy consumption range of 0.10-27.81 $kWh.m^{-3}$ under different operating conditions, while Aljaberi and Hawaas (2023) reported 12.71 $kWh.m^{-3}$ for simultaneous Pb/Cd/Cu removal. Therefore, the energy consumption observed in the present study may be considered technically reasonable for a batch integrated system designed to achieve very high final metal removal from real multi-metal wastewater.

With respect to operating cost, the present system required Rp 43,022 m^{-3}, with adsorbent consumption representing the dominant cost component. A direct numerical comparison with the literature should be interpreted carefully because published costs are influenced by local electricity tariffs, electrode prices, adsorbent prices, and reporting currency. Nevertheless, recent studies suggest that EC operating costs can vary substantially; for example, Bakry et al. (2024) reported a total cost range of 0.02-3.23 $USD.m^{-3}$, whereas Shaker et al. (2023) reported that Ni removal efficiencies of 99.4-99.7% could be achieved at approximately 0.5-0.7 $USD.m^{-3}$ in an EC-only system. Compared with such EC-only studies, the higher cost contribution observed in the present work is reasonably attributable to the addition of the bentonite adsorption stage as a polishing unit. Thus, the proposed EC-Ads configuration offers excellent removal performance and low final residual metal concentrations, but its economic competitiveness would likely be improved further through adsorbent regeneration, reuse, or dosage reduction.

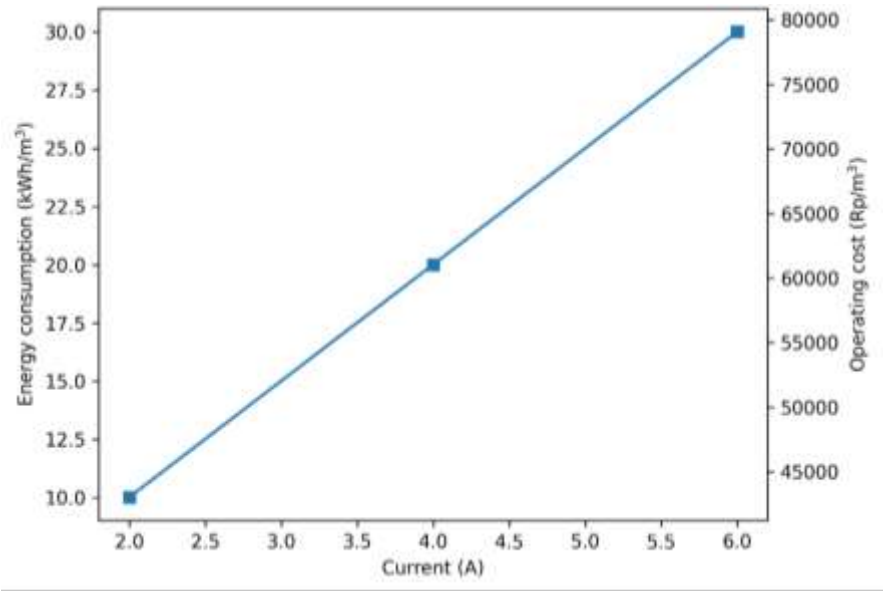

Fig. 13: Relationship between current, energy consumption, and operating cost.

4. CONCLUSIONS

This study confirms that the integrated electrocoagulation–adsorption system using thermally activated bentonite is effective for the simultaneous removal of Pb, Cd, and Ni from real laboratory wastewater. The main contribution of this study is the comparative demonstration that electrocoagulation functions as the primary removal stage, whereas adsorption serves as a polishing step for residual metals at low concentrations.

Evidence from SEM-EDS, FTIR, and ICP-MS characterization indicates that metal removal occurs through complementary mechanisms, namely surface adsorption, coprecipitation, precipitation, and immobilization into the solid phase. From a practical perspective, this system shows strong potential for application in the treatment of multi-metal laboratory wastewater, although adsorbent demand remains the dominant factor in operating costs.

The limitations of this study include the use of a batch system, a one-factor-at-a-time approach, the absence of adsorbent regeneration evaluation, and the lack of investigation into the long-term stability of the sludge. Future research should therefore focus on optimization based on statistical design, continuous-scale testing, adsorbent reusability, and the evaluation of solid residue safety.

Future research should therefore focus not only on statistical optimization design and continuous-scale testing, but also on complete analytical QA/QC reporting, adsorbent reusability, and the evaluation of solid residue safety.

Author Contributions: Muhrinsyah Fatimura: Conceptualization, Methodology, Formal analysis, Investigation, Data curation, Visualization, Writing – original draft.

Tuty Emilia Agustina: Methodology, Project administration, Resources, Supervision, Validation, and Writing –original draft.

Susila Arita: Data curation, Formal analysis, Investigation, Validation.

Elda Melwita: Data curation, Investigation, Resources, Validation.

Rully Masriatini: Data curation, Formal analysis, Investigation, Validation, and Visualization.

Nurlela: Data curation, Investigation, Resources, Validation.

Acknowledgments: The authors gratefully acknowledge the financial support for this research and publication provided by Universitas Sriwijaya under Rector's Decree No. 029/UN9/LPPM.PT/2025 dated September 17, 2025

Declaration of generative AI in scientific writing: The authors declare that ChatGPT, Gemini, and Quill Bot were used exclusively for language editing, translation, and the improvement of figure presentation and overall manuscript readability, under full human supervision. These tools were not involved in the study design, methodology, data collection, data analysis, or scientific interpretation. The authors retain full responsibility for the content and conclusions of this manuscript.

REFERENCES

Al Ali, A., Ouda, M., Naddeo, V., Puig, S. and Hasan, S.W., 2021. Integrated electrochemical–adsorption process for the removal of trace heavy metals from wastewater. *Case Studies in Chemical and Environmental Engineering*, 4, pp. 100147. https://doi.org/10.1016/j.cscee.2021.100147

Aljaberi, F.Y. and Hawaas, Z.A., 2023. Electrocoagulation removal of Pb, Cd, and Cu ions from wastewater using a new configuration of electrodes. *MethodsX*, 10, pp. 101951. https://doi.org/10.1016/j.mex.2022.101951

Aljaberi, F.Y., 2019. Operating cost analysis of a concentric aluminum tubes electrodes electrocoagulation reactor. *Heliyon,* 5, pp. e02307. https://doi.org/10.1016/j.heliyon.2019.e02307

Ammar, M., Yousef, E., Mahmoud, M.A., Ashraf, S. and Baltrusaitis, J., 2023. A comprehensive review of the developments in electrocoagulation for the removal of contaminants from wastewater. *Separations*, 10(6), pp. 337. https://doi.org/10.3390/separations10060337

Anna, B., Kleopas, M., Constantine, S., Anestis, F. and Maria, B., 2015. Adsorption of Cd(II), Cu(II), Ni(II) and Pb(II) onto natural bentonite: Study in mono- and multi-metal systems. *Environmental Earth Sciences*, 73, pp. 5435–5444. https://doi.org/10.1007/s12665-014-3798-0

Bakry, S.A., Matta, M.E., Noureldin, A.M. and Zaher, K., 2024. Performance evaluation of electrocoagulation process for removal of heavy metals from wastewater using aluminum electrodes under variable operating conditions. *Desalination and Water Treatment*, 318, pp. 100396. https://doi.org/10.1016/j.dwt.2024.100396

Bakry, S.A., Matta, M.E., Noureldin, A.M. and Zaher, K., 2024. Performance evaluation of electrocoagulation process for removal of heavy metals from wastewater using aluminum electrodes under variable operating conditions. *Desalination and Water Treatment*, 318, pp. 100396. https://doi.org/10.1016/j.dwt.2024.100396

Bayuo, J., Rwiza, M.J., Choi, J.W., Mtei, K.M., Hosseini-Bandegharaei, A. and Sillanpää, M., 2024. Adsorption and desorption processes of toxic heavy metals, regeneration and reusability of spent adsorbents: Economic and environmental sustainability approach. *Advances in Colloid and Interface Science*, 329, pp. 103196. https://doi.org/10.1016/j.cis.2024.103196

Caixeta, A.L., Silva, A.C.N.D., Silva, S.K.S.D., Dias, M.D.C., Cholant, C.M., Volkmer, T.M., Missio, A.L., Oliveira, A.D.D., Ferrer, M.M., Anwar, Y. and Khan, S., 2025. Sustainable Biosorbent and Biopolymeric Materials for Heavy Metal Adsorption—Advances, Challenges, and Perspectives. *Materials*, 18(20), p.4752.

Ebba, M., Asaithambi, P. and Alemayehu, E., 2021. Investigation on operating parameters and cost using an electrocoagulation process for wastewater treatment. *Applied Water Science*, 11, pp. 175. https://doi.org/10.1007/s13201-021-01517-y

Fan, D., Peng, Y., He, X., Ouyang, J., Fu, L. and Yang, H., 2024. Recent progress on the adsorption of heavy metal ions Pb(II) and Cu(II) from wastewater. *Nanomaterials*, 14. https://doi.org/10.3390/nano14121037

Fei, Y. and Hu, Y.H., 2023. Recent progress in removal of heavy metals from wastewater: A comprehensive review. *Chemosphere*, 335, pp. 139077. https://doi.org/10.1016/j.chemosphere.2023.139077

Fu, F. and Wang, Q., 2011. Removal of heavy metal ions from wastewaters: A review. *Journal of Environmental Management*, 92(3), pp. 407–418. https://doi.org/10.1016/j.jenvman.2010.11.011

Harahap, M.G., Abfertiawan, M.S., Syafila, M., Handajani, M. and Gultom, T.H., 2024. Electrocoagulation for nickel, chromium, and iron removal from mine water using aluminum electrodes. *Heliyon*, 10. https://doi.org/10.1016/j.heliyon.2024.e40784

Hikmat, K., Aziz, H., Mustafa, F.S. and Omer, K.M., 2023. Heavy metal pollution in the aquatic environment: Efficient and low-cost removal approaches to eliminate their toxicity: A review. *RSC Advances*, 13, pp. 17595–17610. https://doi.org/10.1039/D3RA00723E

Huang, C.H., Shen, S.Y., Dong, C.D., Kumar, M. and Chang, J.H., 2020. Removal mechanism and effective current of electrocoagulation for treating wastewater containing Ni(II), Cu(II), and Cr(VI). *Water*, 12(9), pp. 2614. https://doi.org/10.3390/w12092614

Jo, S., Kadam, R., Jang, H., Seo, D. and Park, J., 2024. Recent advances in wastewater electrocoagulation technologies: Beyond chemical coagulation. *Energies*, 17. https://doi.org/10.3390/en17235863

Khan, S.U., Khalid, M., Hashim, K., Jamadi, M.H., Mousazadeh, M., Basheer, F. et al., 2023. Efficacy of electrocoagulation treatment for the abatement of heavy metals: An overview of critical processing factors, kinetic models and cost analysis. *Sustainability*, 15. https://doi.org/10.3390/su15021708

Kim, T., Phu, C., Nguyen, P.L., Viet, T. and Phung, B., 2025. Recent progress in highly effective electrocoagulation-coupled systems for advanced wastewater treatment. *iScience*, 28, pp. 111965. https://doi.org/10.1016/j.isci.2025.111965

Li, W., Zhang, L., Su, T., Luo, X., Xie, X. and Qin, Z., 2025. Carboxymethyl cellulose sodium/bentonite composite adsorbent for Cd(II) adsorption from wastewater. *Advanced Composites and Hybrid Materials*, 8, pp. 119. https://doi.org/10.1007/s42114-024-01185-x

Lu, J., Zhang, P., Li, J., Cao, Y., Zhang, W., Zhang, X. et al., 2024. Mo(VI) removal from water by aluminum electrocoagulation: Cost-effectiveness analysis, main influencing factors, and proposed mechanisms. *Journal of Hazardous Materials*, 461, pp. 132608. https://doi.org/10.1016/j.jhazmat.2023.132608

Magdum, P. and Itankar, N., 2026. Environmental Remediation and Sustainable Approaches to Heavy Metal Removal: A Comprehensive Review of Biosorption Techniques. *Nature Environment and Pollution Technology*, *25*(1), pp.1-21. https://doi.org/10.46488/NEPT.2026.v25i01.B4334

Mao, Y., Zhao, Y. and Cotterill, S., 2023. Examining current and future applications of electrocoagulation in wastewater treatment. *Water*, 15(8), pp. 1455. https://doi.org/10.3390/w15081455

Matra, K., Lerkmahalikit, Y., Prasertkulsak, S., Kongdee, A., Pomthong, R., Thongson, S. et al., 2025. Hybrid RSM–ANN modeling for optimization of electrocoagulation using aluminum electrodes (Al–Al) for hospital wastewater treatment. *Water*, 17, pp. 3003. https://doi.org/10.3390/w17203003

Merrikhpour, H., Mobarakpour, S. and Azimi, S.B., 2022. Adsorption of Cd^{2+}, Cu^{2+}, and Ni^{2+} onto surfactant-modified bentonite. *Desalination and Water Treatment*, 271, pp. 157–165. https://doi.org/10.5004/dwt.2022.28768

Mouedhen, G., Feki, M., Wery, M.D.P. and Ayedi, H.F., 2008. Behavior of aluminum electrodes in electrocoagulation process. *Journal of Hazardous Materials*, 150(1), pp. 124–135. https://doi.org/10.1016/j.jhazmat.2007.04.090

Naldi, N., Hazmi, A., Desmiarti, R. and Emeraldi, P., 2025. Electrocoagulation in Wastewater Treatment: A Comprehensive Review on Parameters and Applications. *Andalas Journal of Electrical and Electronic Engineering Technology*, 5(2), pp.38-49.

Onyenanu, N.R.C.N. and Onyenanu, U.I., 2025. Advanced treatment technologies for heavy metal removal from water and wastewater: A comprehensive review. *International Journal of Advanced Natural Sciences*, pp. 111–131. https://doi.org/10.61424/ijans

Patel, S.K., Shukla, S.C., Natarajan, B.R., Asaithambi, P., Dwivedi, H.K., Sharma, A. et al., 2025. State of the art review for industrial wastewater treatment by electrocoagulation process: Mechanism, cost and sludge analysis. *Desalination and Water Treatment*, 321, pp. 100915. https://doi.org/10.1016/j.dwt.2024.100915

PERMEN, 2014. *Peraturan Menteri Lingkungan Hidup Nomor 5 Tahun 2014: Baku Mutu Air Limbah*. Available at: https://peraturan.bpk.go.id/Details/322442/permen-lh-no-5-tahun-2014 (Accessed April 10, 2026).

PLN.2026.Tariff Adjustment Document. https://www.pln.co.id/tariff-adjustment-document-en. (Accessed May 31, 2026).

Prepilková, V., Poništ, J., Ďuricová, A., Salva, J., Schwarz, M., Samešová, D. et al., 2024. Adsorption of Cd and Mn from neutral mine effluents using bentonite, zeolite, and stabilized dewatered sludge. *Environmental Sciences Europe*, 36, pp. 100. https://doi.org/10.1186/s12302-024-00911-y

Rajaniemi, K., Tuomikoski, S. and Lassi, U., 2021. Electrocoagulation sludge valorization—A review. *Resources*, 10(12), pp. 127. https://doi.org/10.3390/resources10120127

Raji, Z., Karim, A., Karam, A. and Khalloufi, S., 2023. Adsorption of heavy metals: Mechanisms, kinetics, and applications of various adsorbents in wastewater remediation—A review. Waste, 1, pp. 775–805. https://doi.org/10.3390/waste1030046

Sakina, N.A., Sodri, A. and Kusnoputranto, H., 2023. Heavy metals assessment of hospital wastewater during COVID-19 pandemic. *International Journal of Public Health Science*, 12(1), pp. 187–195. https://doi.org/10.11591/ijphs.v12i1.22490

Shaker, O.A., Safwat, S.M. and Matta, M.E., 2023. Nickel removal from wastewater using electrocoagulation process with zinc electrodes under various operating conditions: Performance investigation, mechanism exploration, and cost analysis. *Environmental Science and Pollution Research*, 30(10), pp. 26650-26662. https://doi.org/10.1007/s11356-022-24101-6

Tegladza, I.D., Xu, Q., Xu, K., Lv, G. and Lu, J., 2021. Electrocoagulation processes: A general review about role of electro-generated flocs in pollutant removal. *Process Safety and Environmental Protection*, 146, pp. 169–189. https://doi.org/10.1016/j.psep.2020.08.048

Tran, H.N., 2023. Applying linear forms of pseudo-second-order kinetic model for feasibly identifying errors in the initial periods of time-dependent adsorption datasets. *Water*, 15, pp. 1231. https://doi.org/10.3390/w15061231

Tripathi, A., Dahiya, S. and Mishra, B.K., 2025. Next-generation heavy metal water treatment: A primer on modified capacitive deionization. *Chemical Engineering Journal*, 505, pp. 158844. https://doi.org/10.1016/j.cej.2024.158844

Twizerimana, P. and Wu, Y., 2024. Overview of integrated electrocoagulation–adsorption strategies for the removal of heavy metal pollutants from wastewater. *Discover Chemical Engineering*, 4. https://doi.org/10.1007/s43938-024-00053-w

Ullah, Y., He, X., Fang, Y. and Lu, J., 2025. A review about flocs in electrocoagulation process: Generation, adsorption, transformation, transportation. *Process Safety and Environmental Protection*, 202, pp. 107452. https://doi.org/10.1016/j.psep.2025.107452

Uludag-Demirer, S., Olson, N., Ives, R., Nshimyimana, J.P., Rusinek, C.A., Rose, J.B. et al., 2020. Techno-economic analysis of electrocoagulation on water reclamation and bacterial/viral indicator reductions of a high-strength organic wastewater—anaerobic digestion effluent. *Sustainability*, 12. https://doi.org/10.3390/su12072697

Vareda, J.P., 2023. On validity, physical meaning, mechanism insights and regression of adsorption kinetic models. *Journal of Molecular Liquids*, 376, pp. 121416. https://doi.org/10.1016/j.molliq.2023.121416

Wang, P., Shen, X., Qiu, S., Zhang, L., Ma, Y. and Liang, J., 2024. Clay-based materials for heavy metals adsorption: Mechanisms, advancements, and future prospects in environmental remediation. *Crystals*, 14. https://doi.org/10.3390/cryst14121046

Xu, H., Hu, X., Chen, Y., Li, Y., Zhang, R., Tang, C. et al., 2021. Cd(II) and Pb(II) adsorption on humic acid-iron-pillared bentonite: Kinetics, thermodynamics and mechanism. *Colloids and Surfaces A: Physicochemical and Engineering Aspects*, 612, pp. 126005. https://doi.org/10.1016/j.colsurfa.2020.126005

Yang, X., Li, Y., Gan, M., Chen, Y., Meng, H., Li, L. et al., 2025. Adsorption and desorption effect of modified bentonite on soil heavy metal Pb/Cd and the feasibility assessment of reducing the ecotoxicity. *Environmental Sciences Europe*, 37, pp. 105. https://doi.org/10.1186/s12302-025-01144-3

Yang, X., Zhou, Y., Hu, J., Zheng, Q., Zhao, Y., Lv, G. et al., 2024. Clay minerals and clay-based materials for heavy metals pollution control. *Science of the Total Environment*, 954, pp. 176193. https://doi.org/10.1016/j.scitotenv.2024.176193

Yazıcı Karabulut, B., 2025. Electrochemical coagulant generation via aluminum-based electrocoagulation for sustainable greywater treatment and reuse: Optimization through response surface methodology and kinetic modelling. *Molecules*, 30, pp. 3779. https://doi.org/10.3390/molecules30183779

Yazidi, I., Ziat, K., Bardiji, N.E., Boundati, Y.E., Naji, A., Haskouri, J.E. et al., 2026. Adsorption kinetics, isotherm models, and thermodynamics: A brief review. In: Boutahir, M., Elkhattabi, E.M., Zouini, M., Upadhyay, A., Gadam, H. and

Tyagi, A. (eds), *Artificial Intelligence and Emerging Materials Transition Toward Green Smart Technologies*. Springer Nature: Cham, Switzerland, pp. 93–105. https://doi.org/10.1007/978-3-032-15481-1_8

Zareh, M., Metwally, N. and Abdel-Tawwab, M., 2024. Review of methods of removal of heavy metals from wastewater. *Bulletin of Faculty of Science*, Zagazig University, 2024, pp. 51–58. https://doi.org/10.21608/bfszu.2023.226989.1291